Mathematical modelling of heart rate and blood pressure regulation

Alexander Gibbs

School of Natural and Computational Sciences
Massey University

A thesis presented in partial
fulfilment of the requirements

for the degree of

Master of Science in Mathematics

July 7, 2021

Abstract

A mathematical model of Heart Rate (HR) control has been expanded to include a mechanical model of the heart. The aim is to better understand the significance of Respiratory Sinus Arrhythmia (RSA), a variation of HR with respiration. RSA is found in several species but the physiological benefits and source of it are still under debate. A recently developed model of heart dynamics has been integrated into a model of HR control and gas exchange. HR is assumed to be primarily affected by the parasympathetic signal, with the sympathetic signal taken as a constant in the model. The parasympathetic signal is assumed to be affected by mechanical feedback from the lungs, direct modulation by the respiratory drive, and feedback from the baroreceptors (blood pressure sensors). The inclusion of a mechanical heart model allowed us to better represent the blood pressure in the HR control model and test two hypotheses regarding the function and source of RSA. Our study confirms that the main source of RSA is central modulation of heart rate. However, more work is needed to confirm using this model the hypothesis that RSA minimizes the work done by the heart while maintaining physiological levels of CO_2.

Acknowledgements

I would like to thank my supervisor Alona for her support, patience, and advice during this work.

I would like to thank my wife Victoria for her love, support, and making sure I went for walks.

Contents

List of Figures

List of Tables

Nomenclature

Table 1: Definition of all the variables used in this thesis.

Symbol	Meaning	Units
t	time	s
HR	heart rate	Hz
T_L	heart beat period	s
C_{VN}	integrated cardiac vagal nerve signal	—
G	central-respiratory baroreflex gating function	—
B_R	baroreflex input to cardiac vagal tone	—
MAP	mean arterial pressure	mmHg
A	central respiratory rhythm-generating signal	—
R_p	phrenic nerve signal	—
P_L	pleural pressure	mmHg
q	airflow into the lungs	L/s
V_A	lung volume	L
P_A	total alveolar pressure	mmHg
f_o	alveolar fractional concentration of oxygen	—
f_c	alveolar fractional concentration of carbon dioxide	—
p_o	partial pressure of oxygen	mmHg
p_c	partial pressure of carbon dioxide	mmHg
z	arterial concentration of bicarbonate	mol/L
x_m	diaphragm muscle displacement	m
V_{La}	Left atrium volume	mL
V_{Lv}	Left ventricle volume	mL
V_{Sa}	Systemic arteries volume	mL
V_{Sv}	Systemic veins volume	mL
V_{Ra}	Right atrium volume	mL
V_{Rv}	Right ventricle volume	mL
V_{Pa}	Pulmonary arteries volume	mL
V_{Pv}	Pulmonary veins volume	mL
P_{La}	Left atrium pressure	mmHg
P_{Lv}	Left ventricle pressure	mmHg
P_{Sa}	Systemic arteries pressure	mmHg
P_{Sv}	Systemic veins pressure	mmHg
P_{Ra}	Right atrium pressure	mmHg
P_{Rv}	Right ventricle pressure	mmHg

Continuation of Table 1.

Symbol	Meaning	Units
P_{Pa}	Pulmonary arteries pressure	mmHg
P_{Pv}	Pulmonary veins pressure	mmHg
R_{mv}	Mitral valve resistance	mmHg·s/mL
R_{tv}	Tricuspid valve resistance	mmHg·s/mL
R_{pv}	Pulmonary valve resistance	mmHg·s/mL
R_{av}	Aortic valve resistance	mmHg·s/mL
G_{La}	Force imposed by Left Atrium	mmHg
G_{Ra}	Force imposed by Right Atrium	mmHg
G_{Lv}	Force imposed by Left Ventricle	mmHg
G_{Rv}	Force imposed by Right Ventricle	mmHg

Table 2: Definition of all the parameters and default values used in this thesis. The parameters in the heart rate control model are indicated by [1]. Those indicated by * were found in Chapter 4, the others are those found in [1]. The parameters in the heart model are indicated by [2]. They were estimated to give the results in Chapter 3. The parameters in the lung model are indicated by [3]. They are those found in [1].

Symbol	Meaning	Value	Units
T_{L0}[1]	intrinsic heart beat period of the sinoatrial node	0.6	s
C_{VN0}[1]*	unmodulated central parasympathetic vagal activity	1.6	—
S_M[1]	integrated cardiac sympathetic signal	1	—
S_1[1]*	response frequency of T_L	0.81	Hz
S_2[1]*	response frequency of C_{VN}	0.81	Hz
c_{0-3}[1]	constants affecting the strength of:		
c_0[1]	- parasympathetic input to the heart	1	—
c_1[1]*	- central respiratory signal	1.18	Hz
c_2[1]	- mechanical feedback from the lungs	0.05	$(\text{sL})^{-1}$
k_2[1]	constant affecting the mechanical feedback from the lungs	4.2	L
c_3[1]*	- baroreflex input to the heart	0.74	Hz
δ[1]*	ideal mean arterial pressure	76.1	mmHg
γ[1]	constant affecting the strength of the baroreflex	-0.1945	mmHg^{-1}
k_3[1]	constant affecting the baroreceptor signal	0.5	—
a[1]	constant affecting the slope of the gating function	4	s/L
V_{total}[2]	Total volume of blood	5000	mL
α_{La}[2]	constant affecting the action of the left atrium	1.2	—
A_{La}[2]	constant affecting the action of the left atrium	0.4	—
λ_{La}[2]	constant affecting the action of the left atrium	0.4	mmHg/mL/s
μ_{La}[2]	constant affecting the action of the left atrium	0.4	mL
α_{Ra}[2]	constant affecting the action of the right atrium	1.2	—
A_{Ra}[2]	constant affecting the action of the right atrium	0.4	—
λ_{Ra}[2]	constant affecting the action of the right atrium	0.4	mmHg/mL/s
μ_{Ra}[2]	constant affecting the action of the right atrium	0.4	mL
R_{Pv}[2]	Pulmonary Vein resistance	0.006	mmHg·s/mL
R_{Pa}[2]	Pulmonary Artery resistance	0.01	mmHg·s/mL
R_{Sv}[2]	Systemic Vein resistance	0.01	mmHg·s/mL
R_{Sa}[2]	Aortic valve resistance	0.9	mmHg·s/mL
C_{Pv}[2]	Pulmonary Vein compliance	16.0	mL/mmHg
C_{Pa}[2]	Pulmonary Artery compliance	2.8	mL/mmHg
C_{Sv}[2]	Systemic Vein compliance	80.0	mL/mmHg
C_{Sa}[2]	Aortic valve compliance	1.3	mL/mmHg
R_{opmv}[2]	Open mitral valve resistance	0.02	mmHg·s/mL
R_{optv}[2]	Open tricuspid valve resistance	0.02	mmHg·s/mL
R_{oppv}[2]	Open pulmonary valve resistance	0.006	mmHg·s/mL

Continuation of Table 2.

Symbol	Meaning	Value	Units
$R_{opav}{}^2$	Open aortic valve resistance	0.006	mmHg·s/mL
$V_{unLv}{}^2$	Volume unfilled left ventricle	30.0	mL
$V_{unRv}{}^2$	Volume unfilled right ventricle	30.0	mL
$V_{unPa}{}^2$	Volume unfilled pulmonary artery	155.0	mL
$V_{unPv}{}^2$	Volume unfilled pulmonary vein	415.0	mL
$V_{unSa}{}^2$	Volume unfilled systemic arteries	750.0	mL
$V_{unSv}{}^2$	Volume unfilled systemic veins	2585.0	mL
$G_{minLa}{}^2$	minimum force imposed by left atrium	0.0	mmHg
$G_{minLv}{}^2$	minimum force imposed by left ventricle	0.0	mmHg
$G_{minRa}{}^2$	minimum force imposed by right atrium	0.0	mmHg
$G_{minRv}{}^2$	minimum force imposed by right ventricle	0.0	mmHg
$G_{maxLa}{}^2$	maximum force imposed by left atrium	1.95	mmHg
$G_{maxLv}{}^2$	maximum force imposed by left ventricle	100.3	mmHg
$G_{maxRa}{}^2$	maximum force imposed by right atrium	6.0	mmHg
$G_{maxRv}{}^2$	maximum force imposed by right ventricle	19.9	mmHg
$P_m{}^3$	atmospheric pressure	760	mmHg
$V_o{}^3$	mean alveolar volume	2.5	L
$C_u{}^3$	unit conversion factor	25.426	L/mol
$T_L{}^3$	heart beat period	5/6	s
$p_w{}^3$	water vapor pressure at 37° C	47	mmHg
$f_{om}{}^3$	dry atmospheric O_2 fractional concentration	0.21	—
$f_{cm}{}^3$	dry atmospheric CO_2 fractional concentration	0	—
$V_T{}^3$	tidal volume	0.4	L
$V_D{}^3$	dead-space volume	0.15	L
$V_c{}^3$	capillary volume/heart stroke volume	0.07	L
R^3	airway resistance to flow	1	mmHg· s/L
E^3	lung elastance	2.5	mmHg/L
$T_R{}^3$	respiratory period	5	s
$f_R{}^3$	respiratory frequency	0.2	Hz
$D_o{}^3$	O_2 diffusion capacity	3.5×10^{-4}	L/mmHg/s
$D_c{}^3$	CO_2 diffusion capacity	7.08×10^{-3}	L/mmHg/s
σ^3	O_2 solubility in blood plasma	1.4×10^{-6}	mol/L/mmHg
$\sigma_c{}^3$	CO_2 solubility in blood plasma	3.3×10^{-5}	mol/L/mmHg
$T_h{}^3$	capillary hemoglobin concentration	2×10^{-3}	mol/L
$K_T{}^3$	equilibrium constant in hemoglobin saturation function	10^4	L/mol
$K_R{}^3$	”	3.6×10^6	L/mol
L^3	”	1.712×10^8	—
h^3	capillary H^+ ions concentration	$10^{-7.4}$	mol/L
$r_2{}^3$	dehydration reaction rate	0.12	s^{-1}
$\ell_2{}^3$	hydration reaction rate	1.64×10^5	L/s/mol
$K_E{}^3$	reaction rate acceleration factor due to catalyzing enzyme	$10^{1.9}$	—

Continuation of Table 2.

Symbol	Meaning	Value	Units
k_1[3]	muscle recoil rate	2	s^{-1}
k_p[3]	conversion factor	2.5	mmHg/m
K_n[3]	integrated phrenic activity jump	0.5	—
T_I/T_E[3]	inspiratory to expiratory ratio	0.5	—

Chapter 1

Introduction

Motivation and Aim

Oxygen (O_2) is one of the most vital elements for sustaining life. In humans, other mammals, amhpibians, fish, and many other animals, the cardiorespiratory system consists of a heart and lungs. The lungs are responsible for supplying O_2 to the bloodstream and removing carbon dioxide (CO_2). The heart is responsible for moving O_2-rich blood from the lungs to the rest of the body and returning O_2-poor, CO_2-rich, blood to the lungs. Heart and lung function are tightly regulated in order to supply sufficient O_2-rich blood to the body. One of the most important factors in blood supply is the heart rate (HR) which is influenced by several mechanisms [7].
In particular we are interested in the mechanisms that give rise to respiratory sinus arrhythmia (RSA), a heart rate variability at the frequency of breathing in which HR increases on inspiration and decreases on expiration [5]. RSA is recognised as an indicator of health [8] and there is some evidence that enhancing RSA will help those with heart dysfunction [9]. Ben-Tal et. al. [1] published a mathematical model of HR control accounting for the parasympathetic influence on the heart rate. The model included the effects of lung volume, direct modelation from the respiratory centre, and blood pressure feedback from arterial stretch receptors. The baroreceptor feedback was included by assuming blood pressure is only affected by heart rate. We aim to improve the blood pressure feedback in the HR control model by including a model of the circulation [10] which was designed to study RSA and used a preset function to describe HR variation.

Factors affecting Heart Rate

Heart rate is affected by two nerves, the sympathetic which elevates heart rate, and the parasympathetic which lowers heart rate [11]. Although factors affecting heart rate are generally well understood [11], questions and controversies still exist around the physiological cause [12–16] and physiological function [1, 12, 17–19] of RSA.

Of these two nerves, the parasympathetic is thought to be the main contributer to RSA. The sympathetic signal generally works too slowly to be directly involved in RSA [20], has little activity at rest [21] and RSA persisted in rats when sympathetic drive had been removed [22]. Some investigators [14, 16] agree that RSA is due to direct central respiratory modulation of the parasympathetic signal while others [13, 15] argue RSA is a reflex response to blood pressure changes induced by pressure changes in the thorax which

cause breathing. Menuet et. al. [23] found that neurons involved in generating respiratory rhythms also modulate sympathetic and parasympathetic activity.

The baroreflex helps keep blood pressure constant [24] by sending signals to the central nervous system to lower or increase the heart rate (resulting in lowering or elevating blood pressure respectively) [25] as part of a negative feedback system [26]. Mechanical stretch sensors in the aortic arch and the carotid artery modulate activity in the central nervous system [27], but experiments show that this effect is only effective during expiration [28]. Heart rate reacts quickly to artificially induced changes in blood pressure [24] and since the effort of breathing can change blood pressure, the baroreflex is thought to have an important role in RSA [15].

Physiological Function of RSA

Another controversy is the physiological function of RSA. One hypothesis is that RSA matches perfusion to ventilation within each respiratory cycle and optimises gas exchange [18], but some mathematical modelling did not support this [19], instead hypothesizing that RSA serves to minimise energy expendature of the heart while keeping CO_2 at physological levels. The models in [19] used preset heart rate variations in place of feedback mechanisms in the cardiorespiratory system. A model which included the main features of autonomic heart rate control supported the hypothesis that RSA minimises the work done by the heart to maintain arterial CO_2 levels [1]. Another hypothesis is that RSA stabilises mean arterial blood pressure [17]. Ben-Tal et al. [1] took direct central modulation of the parasympathetic signal as the main mechanism for RSA but included blood pressure feedback from the baroreflex where blood pressure was estimated from the heart rate.

Mathematical Modelling

Mathematical modelling has been used to study aspects of the cardiovascular and nervous systems. In particular we are interested in interactions between the heart and the lungs physically, and through the nervous system.

The pressure changes inside the thorax that cause breathing also have a mechanical effect on the heart and circulation [29]. The effect of the thorax pressure variations on blood pressure was modelled in [30, 31], and [32] used a mathematical model to explain the effect of different breathing manoeuvers on the circulation these did not include heart rate variations. Randall et. al. [33] modelled the effect of the valsalva manoeuver on the heart and also included the effect on the heart rate.

The physical interactions between the heart and the lungs can trigger heart rate changes through the baroreflex. Mathematical models that account for some of the functionality of the baroreflex, but do not include the effect of RSA, have been developed at different levels of complexity. Olufsen et. al. [34] modelled the effect on the heart rate of a change in blood pressure due to a change in posture, some such as [35, 36] model the firing of baroreceptor nerves in response to blood pressure and the resulting change in heart rate. Some models which account for the baroreflex also include the effect of RSA, [37] is a simple model to explore the effect of blood pressure changes in relation to RSA.

Models which are aimed specifically at sudying RSA range from integrate and fire models [38, 39] which use an oscillating threshold to generate RSA, and [40] which modelled

RSA as two coupled oscillators to more detailed models which include [41], which modelled RSA at the level of acetylcholine release in the sinus node, and [42] which included the impact of an emotional stimulus on RSA. Ben-Tal et. al. [19] calculated an optimal heart rate function based on control theory. Csiki and Negoescu [43] developed a model that takes into account respiratory effects on HR through the parasympathetic system. Their work supported the central origin of RSA. Recently, [1] developed a minimal model of RSA with the heart rate mainly affected by the impact of central respiratory drive, lung volume feedback, and baroreflex feedback on the parasympathetic system.

Conclusion

The work by Ben-Tal et.al. [1] did not include a model of all of the mechanics of the heart, and approximated blood pressure feedback with a heart rate. In this work we aim to integrate a mechanical model of the entire circulation [10] into the existing work. This mechanical model of the heart has been designed to study RSA and is able to model the behaviour of the heart with a variable and wide ranging heart rate. Integrating the mechanical model of the heart with the HR control model requires some modifications to the model. We first describe the previous models and the modifications to the models done in this thesis in Chapter 2. We then explore in Chapter 3 the mechanical model of the heart and show how the introduction of pleural pressure to the model affects its outputs. We describe how we chose model parameters in Chapter 4 and in Chapter 5 we use the integrated model to test two hypotheses about the function and source of RSA. Discussions and conclusions of the thesis are provided in Chapter 6.

Chapter 2

Model Development

In the previous chapter we surveyed some of the literature surrounding RSA and heart-lung interactions. In particular, we looked at some of the mathematical models that have been used to study RSA. In this chapter we take a mechanical model of the heart and circulation [10], and a model of heart rate control and breathing [1], and couple them together as a larger integrated model. In coupling the models we apply heart rate control to the heart model, replace an estimate of blood pressure with arterial pressure measured in the heart model, and modify the heart model to include some of the physical effects that breathing has on blood pressure. In this chapter we begin with an overview of the integrated model, and then discuss the details of integrating the models into one.

2.1 Overview of the Integrated Model

Figure 2.1 gives a schematic description of the integrated model that links a model of the heart and circulation based on [10] and a model of heart rate control based on [1] which includes a lung model that was previously published [2, 3].

At the core of the integrated model is the heart rate (Fig. 2.1f), which is affected by the vagus nerve (parasympathetic) and sympathetic nerve (Fig. 2.1 e and i respectively). We

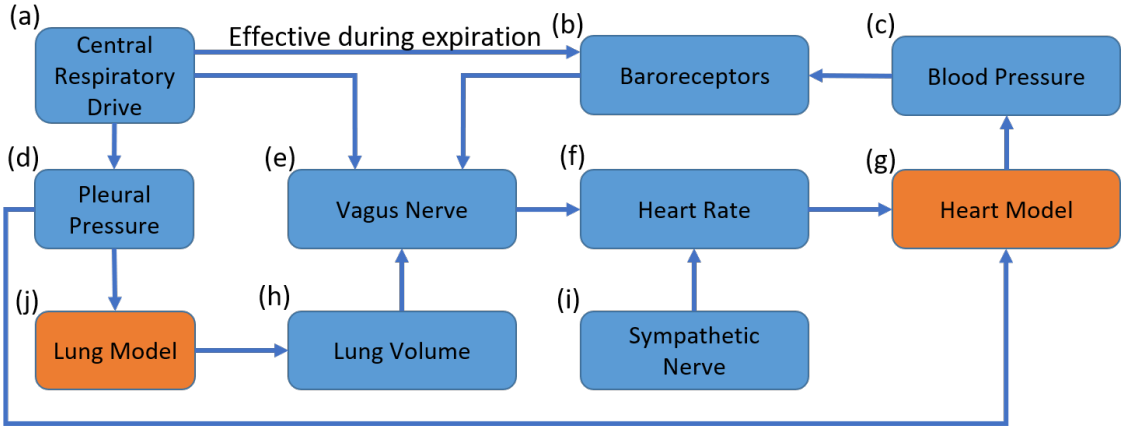

Figure 2.1: Schematic of the integrated heart rate control model showing significant elements of the model and the direction of effects. The orange boxes (j) and (g) represent whole models, which are also described in this section.

assume that the sympathetic nerve acts on a much slower scale than the parasympathetic nerve and therefore take it as constant. We take into account three main factors which affect the parasympathetic signal: central respiratory modulation (Fig. 2.1 a), lung volume (Fig. 2.1 h) taken from the lung model (Fig. 2.1 j), and blood pressure (Fig. 2.1 c) taken from the heart model (Fig. 2.1 g) which is fed back through the baroreceptors (Fig 2.1 b). In addition, the pleural pressure (Fig 2.1 d), which drives lung volume, affects the parts of the heart model which reside inside the chest cavity. We will now describe the different parts of the integrated model in more detail.

2.2 Heart Rate Control Model

The heart rate control model developed in [1] provides a pair of ordinary differential equations for the rate of change of the heart beat period, $T_L(t)$, and the cardiac vagal nerve activity, $C_{VN}(t)$

$$\frac{dT_L}{dt} = -S_1(T_L - T_{L0}) + c_0 C_{VN} - S_M \tag{2.1}$$

$$\frac{dC_{VN}}{dt} = -S_2(C_{VN} - C_{VN0}) - c_1 A + c_2(k_2 - V_A) + c_3 G(qA) B_R(MAP) \tag{2.2}$$

where C_{VN0} is the cardiac vagal nerve activity in the absense of any inputs, and T_{L0} is the intrinsic heart beat period in the absense of the parasympathetic or sympathetic nerves, S_M is the (constant) input of the sympathetic nerve, A is the central respiratory signal, V_A is the lung volume, MAP is mean arterial pressure, and S_1, S_2, c_0, c_1, c_2, k_2, c_3 are constants.

The function $G(qA)$ represents the gating of the baroreceptors during expiration and is given by

$$G(qA) = \frac{1}{1 + e^{a(qA)}} \tag{2.3}$$

where $a > 0$ is a constant. Note that during inspiration $q > 0$ and $G \to 0$ while during expiration $q < 0$ and $G \to 1$. The function $B_R(MAP)$, represents signals from the baroreceptors and is given by

$$B_R(MAP) = \frac{1}{1 + exp\{\gamma(MAP - \delta)\}} - k_3 \tag{2.4}$$

where δ is the ideal mean arterial pressure, γ is a constant affecting the slope of the baroreflex when $MAP = \delta$, and k_3 ensures that $B_R = 0$ when MAP is normal. Eq. 2.4 may be linearised around $MAP = \delta$ to obtain

$$B_R(MAP) = \frac{-\gamma}{4}(MAP - \delta) \tag{2.5}$$

The linearised form was found in [1] to give better agreement with experimental results.

The equations have not changed from [1] except that the source of blood pressure in the baroreflex comes from the heart model. In section 2.4 we give the equations for the heart model and show how we obtain MAP. In section 4.2 we find that for suitable choices of

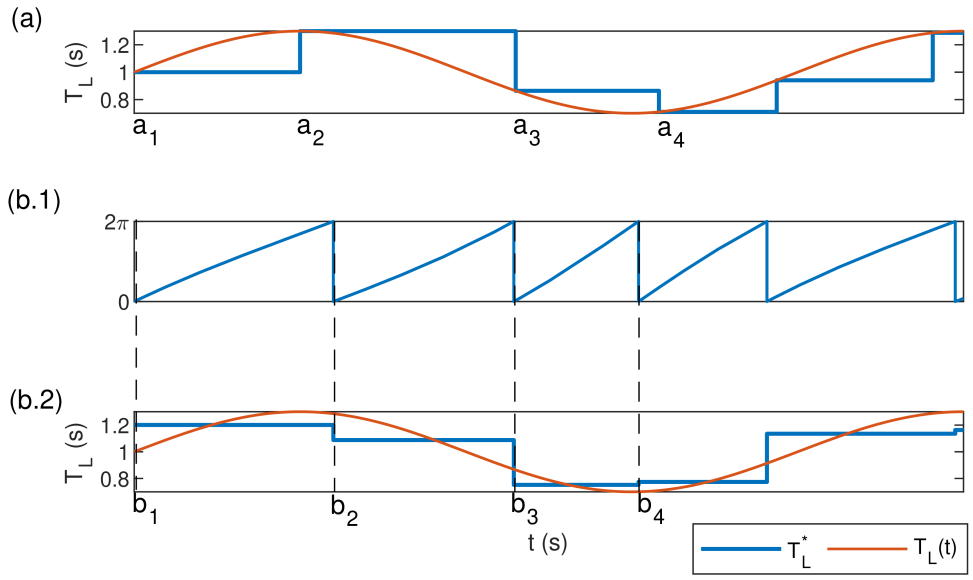

Figure 2.2: Two methods of obtaining a discrete heart beat T_L^* from a continuous heart beat $T_L(t)$. (a) The method used in this thesis. $T_L(t)$ is sampled at the start of a heart beat and when this time lapses, a new value is sampled. (b) The method used in [1]. (b.1) The integral of $2\pi/T_L$, when the integral reaches 2π the integral is reset to zero and a heartbeat occurs. (b.1) The heart beats generated by the integrate and reset method.

parameters, the signal MAP may be replaced by direct input of arterial pressure, denoted by P_{Sa}.

$$B_R(MAP) = \frac{-\gamma}{4}(P_{Sa} - \delta) \tag{2.6}$$

The output of Equation 2.1 is a continuous heart period $T_L(t)$. However, the lung model uses discrete heart beats to calculate gas concentrations in the lungs, and the heart model simulates blood volumes and pressures over discrete heart beats. To find a discrete heart period T_L^*, $T_L(t)$ is sampled at the start of a heart beat to determine the value of T_L^* (Fig. 2.2 a). This gives the time τ for which the model runs $0 \leq \tau \leq T_L^*$ where $\tau = t - t_s$, t is the global time and t_s is the time at the start of a heart beat. The discrete heart period T_L^* was calculated differently in [1] using the integrate and reset mechanism (Fig. 2.2 b). However, this is incompatible with the heart model which requires knowing T_L^* in advance.

2.3 Lung Model

The lung model used in this thesis [2, 3] simulates breathing and gas exchange between air and blood in the lungs. The model consists of a single container in which gas exchange takes place. One side of the container has a moving plate with a spring attached causing air to flow in and out of the lungs (Fig 2.3). At the start of each heart beat it is assumed that a discrete quantity of blood enters the lungs from the heart and gas exchange proceeds

with this quantity of blood (Fig. 2.4). Here we list the 7 differential equations of the lung model.

$$\begin{aligned}
\frac{dP_A}{dt} &= \frac{P_m E}{P_A} Q_A + \frac{dP_L}{dt}, && (2.7)\\
\frac{df_o}{dt} &= \frac{1}{V_A}\left\{D_o\left(p_o - p_{ao}\right) + q_i\left(f_{oi} - f_o\right)\right. \\
&- \left. f_o\left[D_c\left(p_c - p_{ac}\right) + D_o\left(p_o - p_{ao}\right)\right]\right\}, && (2.8)\\
\frac{df_c}{dt} &= \frac{1}{V_A}\left\{D_c\left(p_c - p_{ac}\right) + q_i\left(f_{ci} - f_c\right)\right. \\
&- \left. f_c\left[D_o\left(p_o - p_{ao}\right) + D_c\left(p_c - p_{ac}\right)\right]\right\}, && (2.9)\\
\frac{dp_o}{dt} &= \frac{D_o}{C_u \sigma V_c}\left(1 + \frac{N_0 T_h}{\sigma}\frac{dS}{dp_o}\right)^{-1}\left[f_o\left(P_A - p_w\right) - p_o\right], && (2.10)\\
\frac{dp_c}{dt} &= \frac{D_c}{C_u \sigma_c V_c}\left(p_{ac} - p_c\right) + \frac{K_E \ell_2}{\sigma_c} h z - K_E r_2 p_c, && (2.11)\\
\frac{dz}{dt} &= K_E r_2 \sigma_c p_c - K_E \ell_2 h z, && (2.12)\\
\frac{dx_m}{dt} &= -k_1 x_m + R_p. && (2.13)
\end{aligned}$$

The variables being solved for are: P_A, the total alveolar pressure, f_o and f_c, the alveolar fractional concentrations of O_2 and CO_2 respectively, p_o, p_c, the arterial partial pressures of O_2 and CO_2 respectively, z, the arterial concentration of bicarbonate and x_m, the diaphragm muscle displacement. The values of p_o, p_c and z are initialized every heart beat as the model is integrated forward in time. The "reset" values were taken as $p_o = 40$ mmHg, $p_c = 46$ mmHg and $z = p_c(0)\sigma_c r_2/(h\ell_2)$. The values of p_o and p_c just before the "reset" (Fig. 2.4) represent the blood partial pressures of O_2 and CO_2 respectively when blood leaves the lungs (denoted by p_{oe} and p_{ce} respectively). q_i (appears in Eqs. (2.8) and (2.9)) is the airflow during inspiration ($q_i = 0$ during expiration), f_{oi} and f_{ci} (appear in Eqs. (2.8) and (2.9)) are the inspired concentrations of oxygen and carbon dioxide, respectively and are calculated by the following prescription (replace 'o' by 'c' subscripts to get the rules for f_{ci}):

$$\begin{aligned}
f_{oi} &= f_{om}; \quad V_i > V_D \quad \text{and} \quad (P_m - P_A) > 0,\\
f_{oi} &= f_{od}; \quad V_i \le V_D \quad \text{and} \quad (P_m - P_A) > 0,\\
f_{oi} &= f_o; \quad (P_m - P_A) \le 0, && (2.14)
\end{aligned}$$

where V_D is the dead space volume (the air that remains in the airways after expiration), V_i is the inspired volume of the lungs and is calculated by integrating the airflow during inspiration using the trapezoidal rule, f_{om} is the concentration of oxygen in the mouth, and f_{od} is the concentration of oxygen in the alveolar dead space (calculated as the lung concentration of oxygen at the end of expiration). The other variables appearing in the differential equations are:

$$\begin{aligned}
Q_A &= q + D_c\left(p_c - p_{ac}\right) + D_o\left(p_o - p_{ao}\right), && (2.15)\\
q &= \frac{P_m - P_A}{R}, && (2.16)
\end{aligned}$$

$$
\begin{aligned}
P_L(t) &= P_m - P_{L0} - k_p x_m, && (2.17)\\
V_A &= \frac{P_A - P_L}{E}, && (2.18)\\
p_{ao} &= f_o\left(P_A - p_w\right), && (2.19)\\
p_{ac} &= f_c\left(P_A - p_w\right), && (2.20)\\
S(p_o) &= \frac{LK_T\sigma p_o\left(1+K_T\sigma p_o\right)^3 + K_R\sigma p_o\left(1+K_R\sigma p_o\right)^3}{L\left(1+K_T\sigma p_o\right)^4 + \left(1+K_R\sigma p_o\right)^4}, && (2.21)
\end{aligned}
$$

where Q_A is the net flux of gas into the lungs, q is the airflow, P_L is the pleural pressure (see fig. 2.1 d and 2.3), V_A is the alveolar volume, p_{ao} and p_{ac} are the alveolar partial pressures of O_2 and CO_2 respectively and $S(p_o)$ is the Hemoglobin saturation function.

The activity of the central respiratory signal (Fig 2.1 a) is modeled as a square wave:

$$
A = \begin{cases} A_t & \text{if} \quad \mathrm{mod}(t, T_R) \le T_I \\ A_b & \text{if} \quad T_I < \mathrm{mod}(t, T_R) \le T_E, \end{cases} \tag{2.22}
$$

In all of our simulations $A_t = 0.43$ and $A_b = 0.28$. The diaphragm muscle is controlled by the ramp signal R_p (see Eq. (2.13) and figure 2.3) and is calculated from A in the following way:

$$
R_p(t) = \begin{cases} K_n & \text{if A(t)}\geq T_{r1} \text{ and } R_p(t-\Delta t) <= 0.001 \\ I_p & \text{if A(t)}\geq T_{r1} \text{ and } R_p(t-\Delta t) > 0.001 \\ 0 & \text{if A(t)}< T_{r1} \end{cases} \tag{2.23}
$$

where $I_p = \left[A(t) - I_l R_p(t-\Delta t)\right]\Delta t + R_p(t-\Delta t)$ [1]. In all of our simulations $T_{r1} = 0.35$.

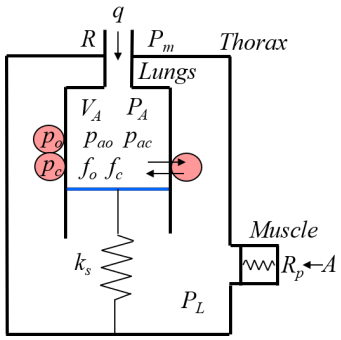

Figure 2.3: Schematic of the lung model [2, 3] (see also figure 2.1 j). The lung is assumed to consist of one container in which gas exchange takes place, with a moving plate attached to a spring. V_A is the total lung volume, P_A is the alveolar pressure, P_m is atmospheric pressure, P_L is pleural pressure (the pressure inside the chest cavity), q is air flow, R is the overall resistance of the conducting airways, k_s is a spring constant (spring compression represents lung expansion; the lung elastance, E, is equivalent to k_s/s^2 where s is the area of the moving plate indicated by the blue line). f_o and f_c are the alveolar concentrations of oxygen and carbon dioxide respectively. p_{ao} and p_{ac} are the alveolar partial pressures of oxygen and carbon dioxide, respectively. p_o and p_c are the blood partial pressures of oxygen and carbon dioxide, respectively. R_p, controlled by central respiratory drive A, is a signal from the brainstem that activates the muscle.

The meaning and values of all the parameters in this model are given in Table 2. These

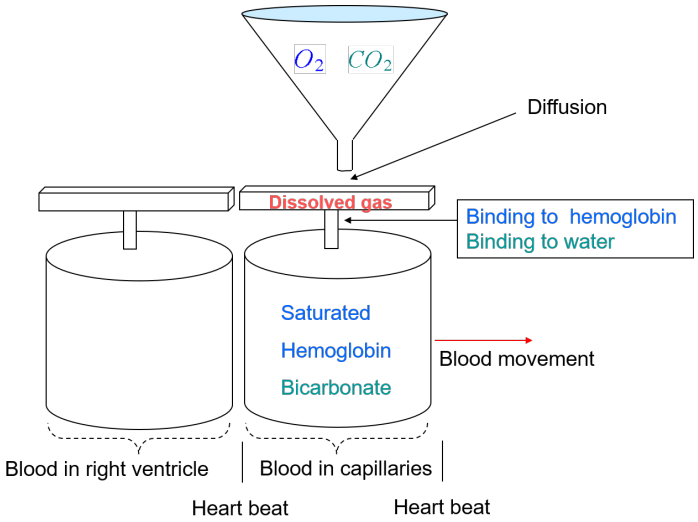

Figure 2.4: Conveyor model approximating blood flow and gas exchange in the lungs [2, 3]. It is assumed that when the heart beats, all of the blood in the right ventricle of the heart is transferred into the lungs and gas concentrations are reset to given starting values.

parameters are typical for humans (i.e. represent an average subject) and are used as the default if an explicit value is not mentioned for a specific simulation. All values are taken from [3].

2.4 Heart and Circulation Model

The heart model used in this thesis calculates the volumes and pressures of blood in the heart and other parts of the circulation. The model consists of eight compartments: the four chambers of the heart, two compartments representing the pulmonary veins and arteries, and two compartments representing the systemic veins and arteries. The compartments are modelled as an elastic containers connected by resistances, the muscle contraction of the chambers of the heart is modelled as an external force, and the heart valves are modelled by variable resistances. The model is based on [10]. Here we describe the 9 ordinary differential equations of the heart model.

$$\frac{dV_{La}}{dt} = \frac{P_{Pv} - P_{La}}{R_{Pv}} - \frac{P_{La} - P_{Lv}}{R_{mv}} \tag{2.24}$$

$$\frac{dP_{La}}{dt} = \begin{cases} \alpha_{La} E_{minLa} \frac{dV_{La}}{dt} + \frac{dG_{La}}{dt} + \lambda_{La}(V_{La} - \mu_{La}) & \frac{dV_{La}}{dt} < 0.0 \\ A_{La} E_{minLa} \frac{dV_{La}}{dt} + \frac{dG_{La}}{dt} & \frac{dV_{La}}{dt} \geq 0.0 \end{cases} \tag{2.25}$$

$$\frac{dV_{Lv}}{dt} = \frac{P_{La} - P_{Lv}}{R_{mv}} - \frac{P_{Lv} - P_{Sa}}{R_{av}} \tag{2.26}$$

$$\frac{dV_{Sa}}{dt} = \frac{P_{Lv} - P_{Sa}}{R_{av}} - \frac{P_{Sa} - P_{Sv}}{R_{Sa}} \tag{2.27}$$

$$\frac{dV_{Ra}}{dt} = \frac{P_{Sv} - P_{Ra}}{R_{Sv}} - \frac{P_{Ra} - P_{Rv}}{R_{tv}} \tag{2.28}$$

$$\frac{dP_{Ra}}{dt} = \begin{cases} \alpha_{Ra} E_{minRa} \frac{dV_{Ra}}{dt} + \frac{dG_{Ra}}{dt} + \lambda_{Ra}(V_{Ra} - \mu_{Ra}) & \frac{dV_{Ra}}{dt} < 0.0 \\ A_{Ra} E_{minRa} \frac{dV_{Ra}}{dt} + \frac{dG_{Ra}}{dt} & \frac{dV_{Ra}}{dt} \geq 0.0 \end{cases} \tag{2.29}$$

$$\frac{dV_{Rv}}{dt} = \frac{P_{Ra} - P_{Rv}}{R_{tv}} - \frac{P_{Rv} - P_{Pa}}{R_{pv}} \tag{2.30}$$

$$\frac{dV_{Pa}}{dt} = \frac{P_{Rv} - P_{Pa}}{R_{pv}} - \frac{P_{Pa} - P_{Pv}}{R_{Pa}} \tag{2.31}$$

$$\frac{dV_{Pv}}{dt} = \frac{P_{Pa} - P_{Pv}}{R_{Pa}} - \frac{P_{Pv} - P_{La}}{R_{Pv}} \tag{2.32}$$

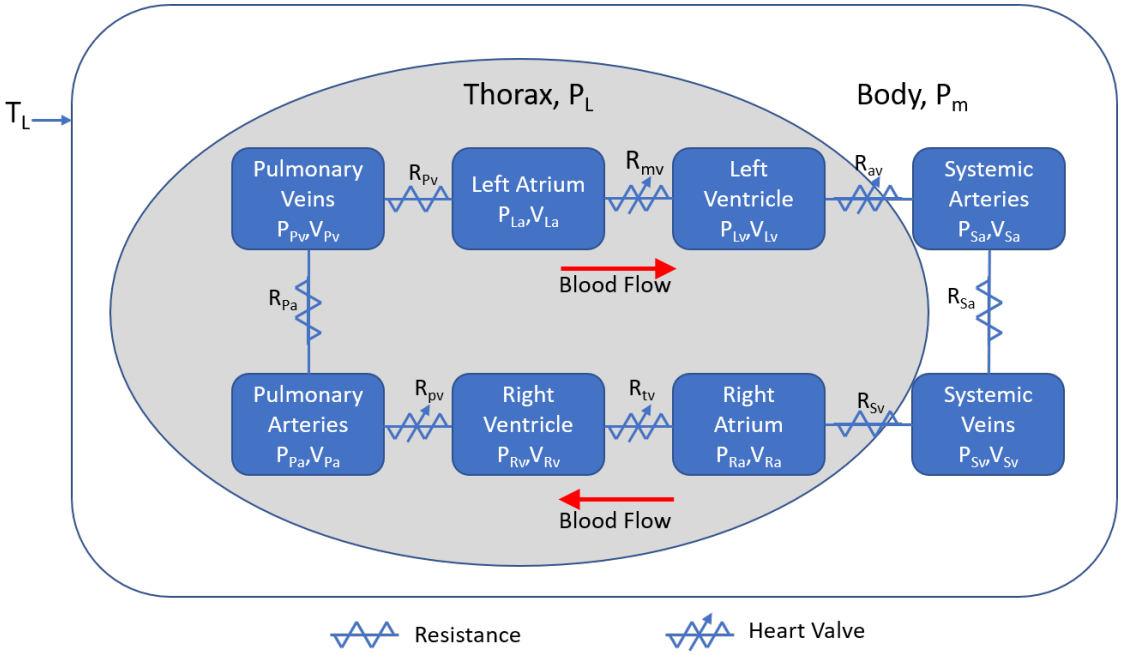

Figure 2.5: Schematic of the model of the heart and circulation. The model consists of 4 compartments representing the heart chambers: Right Atrium, Right Ventricle, Left Atrium and Left Ventricle, and 4 compartments lumping together the pulmonary and systemic arteries and veins. Each compartment has an associated Volume V_x and Pressure P_x, where x is one of Ra, Rv, La, Lv, Pa, Pv, Sa, Sv. Compartments are linked by constant resistances: R_{Pa}, R_{Pv}, R_{Sa}, and R_{Sv} representing the resistance to blood flow in the blood vessels, or pressure dependant resistances R_{mv}, R_{av}, R_{tv}, R_{pv}, representing the mitral valve, aortic valve, tricuspid valve and pulmonary valve respectively. The red arrows indicate the direction of blood flow and the shaded area indicates the compartments of the heart model which are affected by pleural pressure, P_L. P_m is atmospheric pressure and T_L is the heart period given as an input from Equation 2.1.

The variables being solved for are: V_{La}, the volume of the left atrium, P_{La}, the pressure of the left atrium, V_{Lv}, the volume of the left ventricle, V_{Sa}, the volume in the systemic arteries, V_{Ra}, the volume in the right atrium, P_{Ra}, the pressure in the right atrium, V_{Rv}, the volume of the right ventricle, V_{Pa}, the volume in the pulmonary arteries, and V_{Pv}, the volume in the pulmonary veins. R_{mv}, R_{av}, R_{Sa}, R_{Sv}, R_{tv}, R_{pv}, R_{Pa}, R_{Pv} are the resistances of the mitral valve, aortic valve, systemic arterial resistance, systemic venous resistance, tricuspid valve, pulmonary valve, pulmonary arterial resistance, and pulmonary

venous resistance respectively. Equations 2.25 and 2.29 are a new hypothesis from [10] that represent the difference in properties of the atria during contraction and relaxation. The other volumes and pressures in the model are given by:

$$
\begin{aligned}
V_{Sv} &= V_{total} - (V_{La} + V_{Lv} + V_{Ra} + V_{Rv} + V_{Sa} + V_{Pa} + V_{Pv}) && (2.33)\\
P_{Sa} &= (V_{Sa} - V_{unSa})/C_{Sa} && (2.34)\\
P_{Sv} &= (V_{Sv} - V_{unSv})/C_{Sv} && (2.35)\\
P_{Pa} &= (V_{Pa} - V_{unPa})/C_{Pa} && (2.36)\\
P_{Pv} &= (V_{Pv} - V_{unPv})/C_{Pv} && (2.37)\\
P_{Lv} &= E_{minLv}(V_{Lv} - V_{uLv}) + G_{Lv} && (2.38)\\
P_{Rv} &= E_{minRv}(V_{Rv} - V_{uRv}) + G_{Rv} && (2.39)
\end{aligned}
$$

where V_{Sv} is the volume in the systemic veins and P_{Sa}, P_{Sv}, P_{Pa}, P_{Pv}, P_{Lv}, P_{Rv} are the pressures in the systemic arteries, systemic veins, pulmonary arteries, pulmonary veins, left ventricle and right ventricle respectively. The 4 main valves in the heart are modelled by varying the resistances as follows:

$$
\begin{aligned}
R_{mv} &= R_{cl} - \frac{R_{cl} - R_{opmv}}{1.0 + exp(\beta_{mv}(P_{La} - P_{Lv}))} && (2.40)\\
R_{tv} &= R_{cl} - \frac{R_{cl} - R_{optv}}{1.0 + exp(\beta_{tv}((P_{Ra} - P_{Rv}))} && (2.41)\\
R_{pv} &= R_{cl} - \frac{R_{cl} - R_{oppv}}{1.0 + exp(\beta_{pv}((P_{Rv} - P_{Pa}))} && (2.42)\\
R_{av} &= \begin{cases} R_{cl} - \frac{R_{cl} - R_{opav}}{(1.0 + exp(\beta_{av}((P_{Lv} - P_{Sa})))} & f_{hys} = 1 \\ R_{cl} - \frac{R_{cl} - R_{opav}}{(1.0 + exp(\beta_{av}((P_{Lv} - P_{Sa} + 4.5)))} & f_{hys} = 0 \end{cases} && (2.43)\\
f_{hys}(t + \Delta t) &= \begin{cases} 0 & f_{hys}(t) = 1 \text{ and } P_{Lv} - P_{Sa} > 7 \\ 1 & f_{hys}(t) = 0 \text{ and } P_{Lv} - P_{Sa} < -30 \\ f_{hys}(t) & otherwise \end{cases} && (2.44)
\end{aligned}
$$

Where f_{hys} is a state variables describing hysteresis in the opening and closing of the aortic valve. Modelling the aortic valve resistance with hysteresis allows us to mimic the back flow of blood seen in measurements.

The function G_x, where x is La or Ra, describe the forces imposed on the left and right atrium respectively. The rate of change of these is given by:

$$
\frac{dG_x}{dt} = \begin{cases} \frac{(G_{max} - G_{min})\pi \sin\left(\pi \frac{\tau}{T_M}\right)}{2T_M} & \tau \leq T_M \\ \frac{-(G_{max} - G_{min})\pi \sin\left(\frac{\pi(\tau - T_M)}{T_R}\right)}{2T_R} & T_M \leq \tau \leq T_M + T_R \\ 0 & \tau \leq T_M + T_R \end{cases} \quad (2.45)
$$

Where $T_M = 1.2d$, and $T_R = 0.6d$ describe the timing of contraction and relaxation of the atrium, $d = \frac{d_1}{1 + exp(d_2 + d_3 T_L^*)} - d_4$ (d_{1-4} are constants) describes the delay between atrial and ventricular contractions. The maximum and minimum forces exerted are given by $G_{min} = G_{minLa}$ and $G_{max} = G_{maxLa}$ for the left atrium and $G_{min} = G_{minRa}$ and $G_{max} = G_{maxRa}$ for the right atrium.

The function G_x, where x is Lv or Rv, describe the forces imposed on the left and right atrium respectively and are given by:

$$G_x = \begin{cases} G_{min} & \tau \leq d \\ G_{min} + \frac{(G_{max}-G_{min})(1-\cos\left(\frac{\pi(\tau-d)}{T_M}\right))}{2} & d \leq \tau \leq d + T_{Mv} \\ G_{min} + \frac{(G_{max}-G_{min})(1+\cos\left(\frac{\pi(\tau-d-T_M)}{T_R}\right))}{2} & d + T_{Mv} \leq \tau \leq d + T_{Mv} + T_{Rv} \\ G_{min} & \tau \leq d + T_{Mv} + T_{Rv} \end{cases} \tag{2.46}$$

Where $T_{Mv} = 0.67 * (0.39 * (T_L^*)^{(1/3)})$, $T_{Rv} = 0.33 * (0.39 * (T_L^*)^{(1/3)})$ describe the timing of contraction and relaxation of the ventricle. The maximum and minimum forces exerted are given by $G_{min} = G_{minLv}$ and $G_{max} = G_{maxLv}$ for the left ventricle and $G_{min} = G_{minRv}$ and $G_{max} = G_{maxRv}$ for the right ventricle.

Mean Arterial Pressure and Stroke Volume

The heart model gives access to systemic arterial pressure, P_{Sa}, in the heart model, which we assume is a measure of both aortic arch and carotid sinus blood pressure and the pressure signal of interest to the baroreceptors. Experimental data is often given in terms of mean arterial pressure, which we derive from P_{Sa} using the integral

$$MAP = \frac{1}{T_L^*} \int_0^{T_L^*} P_{Sa} d\tau \tag{2.47}$$

Recall that T_L^* is the duration of a heart beat (see figure 2.2). At the end of each heart beat the result of the integral is held as MAP (see figure 2.6 below), meaning that this method gives a natural delay of 1 heart beat in the MAP signal.

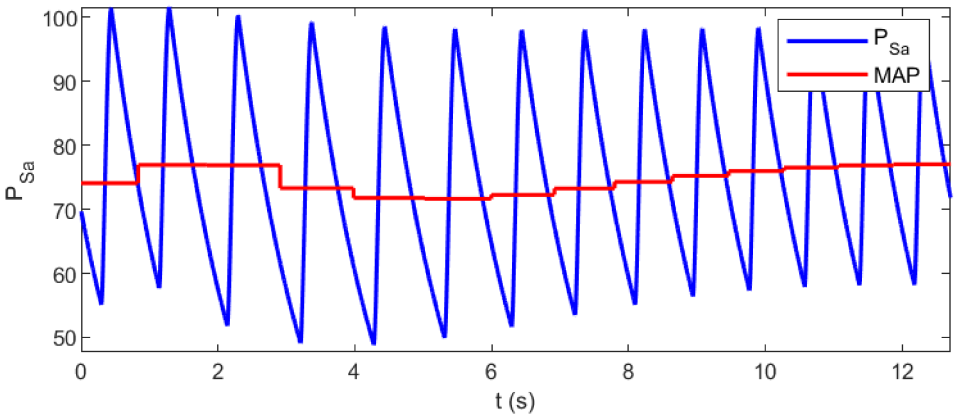

Figure 2.6: Generating mean arterial pressure signal from the arterial pressure using Equation 2.47. Every time the heart beats the integral is reset and the value of MAP is updated.

Another output of the heart model of interest is the right stroke volume, the volume of blood ejected from the right ventricle during a heart beat. The model of the lungs assumed the stroke volume (V_c in Equations 2.11 and 2.12) to be constant, but with the

inclusion of the heart model we can change this. The simplest way to account for the changing stroke volume is to replace the parameter V_c with the volume of blood that exited the right ventricle during a heart beat. At the end of each heart beat, the value of V_c is updated as a result of the integral

$$V_c = \int_0^{T_L^*} \frac{P_{Rv} - P_{Pa}}{R_{pv}} d\tau \tag{2.48}$$

2.5 Physical Effects

Alongside the nervous system effects, there exist significant physical effects of breathing on the heart. Two such effects are the influence of pleural pressure on the heart, and a change of resistance in blood vessels when blood pressure changes. Both of these physical effects can change cardiac output and blood pressure, which can in turn influence the control of heart rate. In this section we consider how these effects can be included in the model.

2.5.1 Pressure Differences

The heart model assumes that the pressures in all eight compartments are relative to atmospheric pressure. However, pressure changes inside the thorax impose additional pressures on the parts of the circulation within the thorax [11, 29]. We assume the six compartments within the thorax are exposed to pleural pressure while those outside the thorax are exposed to atmospheric pressure. In the closed system all pressures responsible for fluid flow should be relative to the same reference pressure which we take as atmospheric pressure. One possible extension beyond the scope of this work is to introduce an additional compartment between pulmonary arteries and veins representing the capillaries which are exposed to alveolar pressure. By way of example for the Left Ventricle we now describe how we can account for the different environments of the compartments and keep pressures expressed relative to atmospheric pressure.

In the original heart model, pressure relative to atmospheric pressure in the left ventricle is given by Equation 2.38. We make the substitution $P_{Lv} = P_{Lv}^* - P_m$, where P_{Lv}^* is the absolute pressure in the left ventricle, to obtain

$$P_{Lv}^* - P_m = E_{minLv}(V_{Lv} - V_{uLv}) + G_{Lv} \tag{2.49}$$

Now, in figure 2.5 the pressure outside the left ventricle is the pleural pressure, rather than atmospheric pressure. To account for pleural pressure we replace P_m with P_L and P_{Lv}^* with $\hat{P}_{Lv}^*$, where $\hat{P}_{Lv}^*$ is the absolute pressure in the left ventricle under the influence of pleural pressure, to obtain a new equation

$$\hat{P}_{Lv}^* - P_L = E_{minLv}(V_{Lv} - V_{uLv}) + G_{Lv} \tag{2.50}$$

Note that P_L in the lung model is absolute pressure. We define the relative pressure in the Left Ventricle accounting for pleural pressure as $\hat{P}_{Lv} = \hat{P}_{Lv}^* - P_m$ so Equation 2.50

can be rewritten as

$$\hat{P}_{Lv} = E_{minLv}(V_{Lv} - V_{uLv}) + G_{Lv} + P_L - P_m \quad (2.51)$$
$$= P_{Lv} + P_L - P_m \quad (2.52)$$

The compartments in the thorax can be treated similarly allowing us to write the pressures under the influence of pleural pressure $\hat{P}_x$ in terms of the pressures P_x in the original heart model, where x means one of La, Lv, Ra, Rv, Pa, Pv, Sa, or Sv.

$$\hat{P}_{La} = P_{La} + P_L - P_m \quad (2.53)$$
$$\hat{P}_{Lv} = P_{Lv} + P_L - P_m \quad (2.54)$$
$$\hat{P}_{Ra} = P_{Ra} + P_L - P_m \quad (2.55)$$
$$\hat{P}_{Rv} = P_{Rv} + P_L - P_m \quad (2.56)$$
$$\hat{P}_{Pa} = P_{Pa} + P_L - P_m \quad (2.57)$$
$$\hat{P}_{Pv} = P_{Pv} + P_L - P_m \quad (2.58)$$
$$\hat{P}_{Sa} = P_{Sa} \quad (2.59)$$
$$\hat{P}_{Sv} = P_{Sv} \quad (2.60)$$

2.5.2 Pulmonary Resistance

It is known that the resistance to blood flow in the pulmonary circulation is sensitive to changes in blood pressure [44, 45]. Resistance to blood flow decreases with increased diameter of a blood vessel [11] and since the diameter of a blood vessel increases with pressure, we can assume that the resistance will decrease in response to an increased blood pressure. During the lowered pressures caused by inhalation this sensitivity could produce a significant interaction between the heart and lungs affecting stroke volume, cardiac output, and blood pressure. The blood vessels inside the lungs are complex, so we seek a simplistic model of the resistance response to change in pressure and investigate the possibility that pulmonary blood vessel resistance due to changes in pressure can cause significant effects in the model. During trials in modelling, a periodic variation of pulmonary artery resistance R_{Pa} caused left and right stroke volumes and cardiac outputs to oscillate out of phase, in agreemeant with some literature [46], indicating that R_{Pa} could play a role in the interaction between the heart and the lungs.

Smaller blood vessels have greater resistance to blood flow, so we estimate blood pressure in the capillaries of the lung P_{cap} as the average of pulmonary arterial (P_{Pa}) and venous (P_{Pv}) blood pressures

$$P_{cap} = \frac{P_{Pa} + P_{Pv}}{2} = \frac{V_{Pa} - V_{unPa}}{2C_{Pa}} + \frac{V_{Pv} - V_{unPv}}{2C_{Pv}} \quad (2.61)$$

To satisfy the requirement that resistance decreases with increased pressure, we estimate the function for pressure sensitive resistance $\hat{R}_{Pa}$ as a function of mean pressure P_{cap} as

$$\hat{R}_{Pa}(P_{cap}) = R_{Pa} \exp\left(k_{Pa}\left(P_{cap} - P_0\right)\right) \quad (2.62)$$

where R_{Pa} is the normal resistance at average blood pressure P_0, and k_{Pa} determines the

strength of the resistance change. We may vary the resistance either without or with the mechanical influence of the lungs (i.e. pleural pressure). In the absence of the influence of the lungs, only heart rate would cause resistance to vary through pressure changes. When the influence of the lungs is included, both the heart rate and the pleural pressure would cause resistance to vary through pressure changes.

2.6 Summary

In this chapter we have described a model which integrates previously published models of heart rate control, gas exchange in the lungs, and a model of the pressures and volumes in the heart chambers and the circulation. The model consists of 18 differential equations: 2.1 and 2.2, 2.8 to 2.13, and 2.24 to 2.32. In developing this model we have:

- included calculated, rather than estimated, blood pressure feedback in the HR control model;
- replaced a given heart beat period in the heart model with a calculated heart beat period;
- applied the physical effect of the pleural pressure changes to the heart model;
- applied the effect of variable blood vessel resistance in the lungs to the heart model.

Chapter 3

Output of the Heart Model

In this chapter we investigate the heart model in isolation at a constant heart rate, and show how the modifications we introduced to the heart model affect its output. We show that applying both a static and oscillating pleural pressure modifies the volume distribution and pressure levels in the compartments of the heart model. Under the current assumptions, the modification of the resistance of the blood vessels in the lungs does not cause as significant an effect as the pleural pressure.

3.1 Original Heart Model

Figures 3.1 to 3.2 give steady-state outputs of the heart model at heart rates of 72 bpm and 90 bpm. In the heart model at 72bpm, the distribution of blood volume and blood pressure is a fair approximation of real values. The total volume in the heart ranges from 240mL to 320mL, 4.8% to 6% of blood total volume, compared to 7% indicated by [47], the total volume in the systemic arteries ranges from 824mL to 877mL, 16.4% to 17.5% of blood total volume, compared to 20% indicated by [47], the total volume in the systemic veins ranges from 3060mL to 3080mL, 61.2% to 61.6% of total blood volume, compared to 64% indicated by [47], and the total volume in the pulmonary circulation ranges from 780mL to 833mL,15.6% to 16.6% of total blood volume, compared to 9% indicated by [47]. The pressure-volume (P-V) loops in the four chambers of the heart (see Figure 3.3) are good approximations of real findings, in particular the figure-of-8 shape of the loop in the atria [48]. We used parameters given in Table 2 which were estimated during the development of the models in [10] to represent physiological values of volume and pressure in humans.

3.2 Impact of Physical Effects on the Heart Model

In chapter 2 we introduced modifications to some of the pressure signals (2.5.1) and blood vessel resistances (2.5.2) of the heart model to account for some of the physical interactions between the heart and the lungs. In this section we consider the impact of these physical effects on the pressures and volumes of the compartments in the heart model at a constant heart rate of 72bpm. In later sections we combine these effects with heart rate control through the baroreflex.

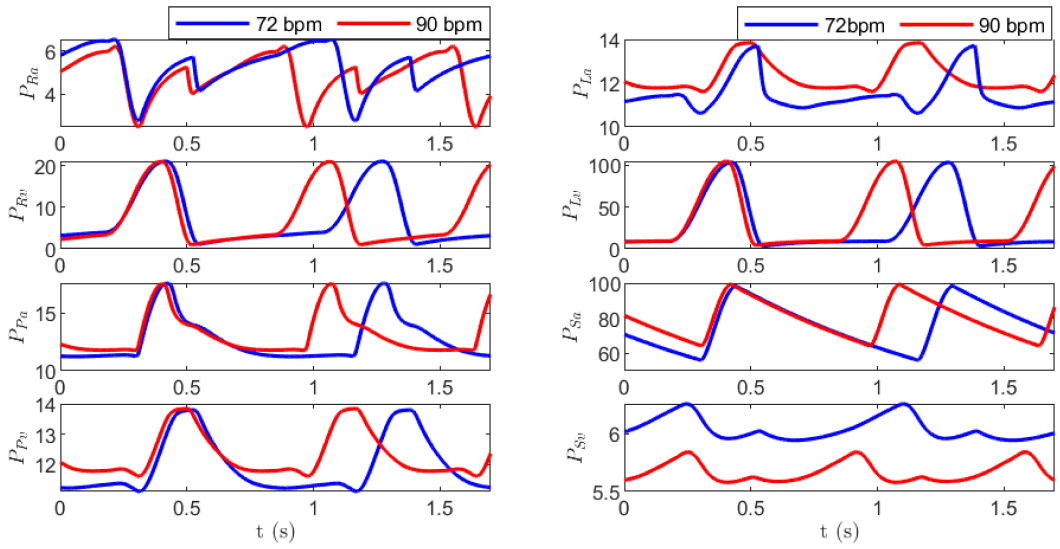

Figure 3.1: Pressures (in mmHg) in the eight compartments of the heart model at 72 bpm and 90 bpm using the model described by Equations 2.24 to 2.32.

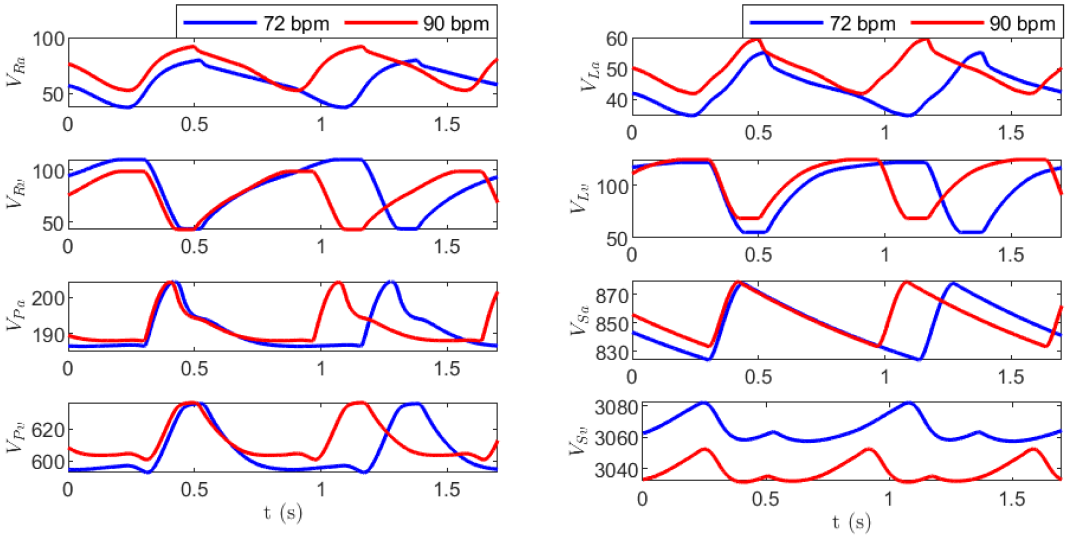

Figure 3.2: Volumes (in mL) in the eight compartments of the heart model at 72bpm and 90 bpm using the model described by Equations 2.24 to 2.32.

3.2.1 Impact of Pleural Pressure

In this section we show that applying pleural pressure redistributes blood and adjusts pressure in the heart model. The pleural pressure signal from the lung model is in two components, a steady negative component of about -6mmHg and an oscillatory component with an amplitude of approximately 2mmHg. We use equations 2.24 to 2.32 with pressures given by equations 2.53 to 2.60 where we use artificially generated P_L signals rather than those generated in the lung model. Figures 3.4 to 3.6 show the effect on the heart model

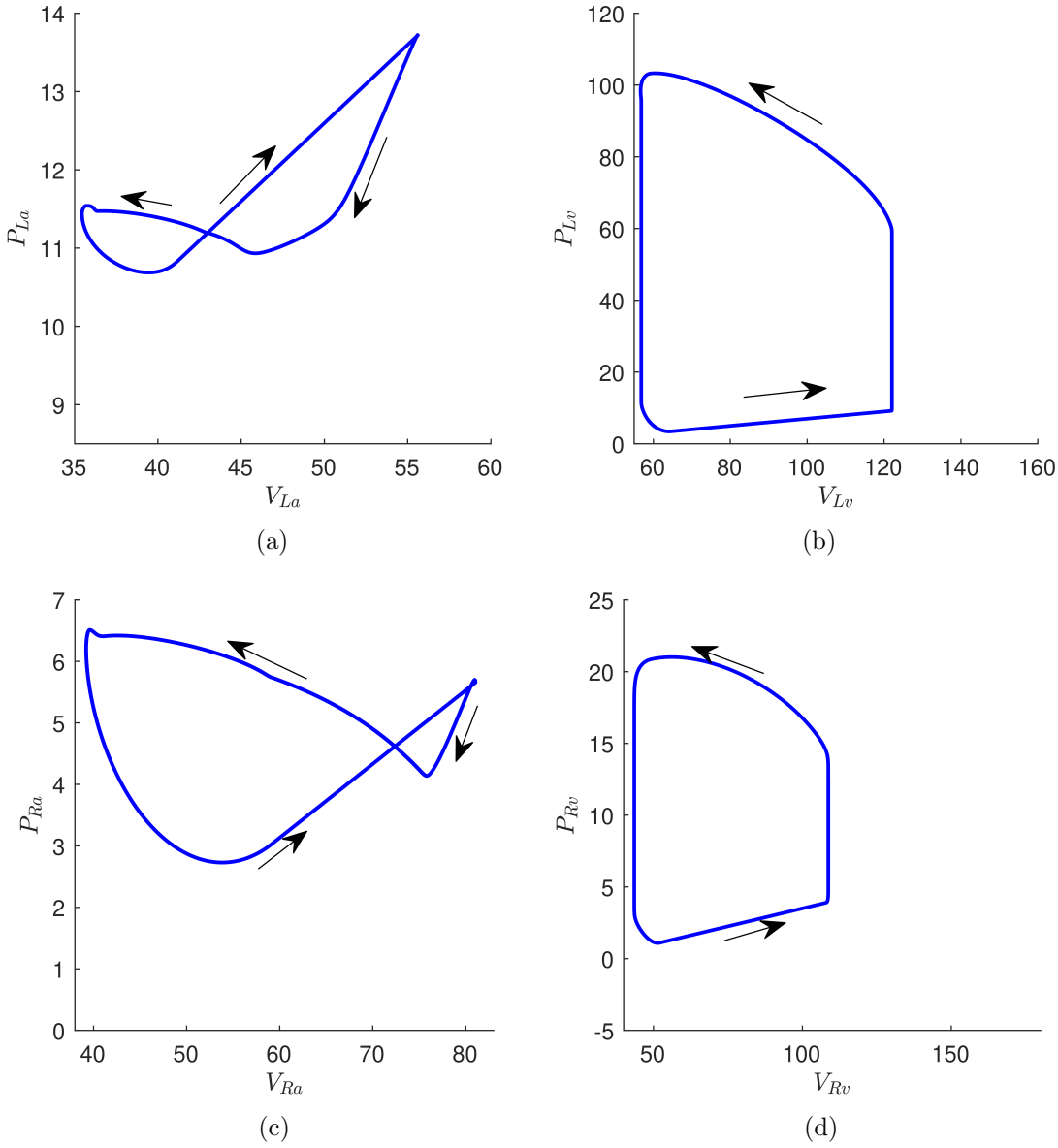

Figure 3.3: P-V (mmHg-mL) loops of left atrium (a), left ventricle (b), right atrium (c) and right ventricle (d) at 72bpm.

of the sudden onset of a constant pleural pressure of -6mmHg. The sudden pressure imbalance causes a momentary increase in the right stroke volume and cardiac output and a decrease in the left stroke volume and cardiac output as blood is drawn into the chest cavity from the body. After about 6 seconds, the heart model reaches a new steady state with increased blood volume in the chest cavity compartments and reduced blood volume in the body. All of the blood pressures in the 8 compartments are reduced relative to atmospheric pressure. In particular *MAP* is reduced, which will induce HR changes when HR control from the baroreflex is introduced but stroke volume and cardiac output do not change at steady state.

Figures 3.7 to 3.8 show the effect on the heart model of an oscillating pleural pressure with an amplitude of 2mmHg and a period of 5s. The oscillating pressure causes volume

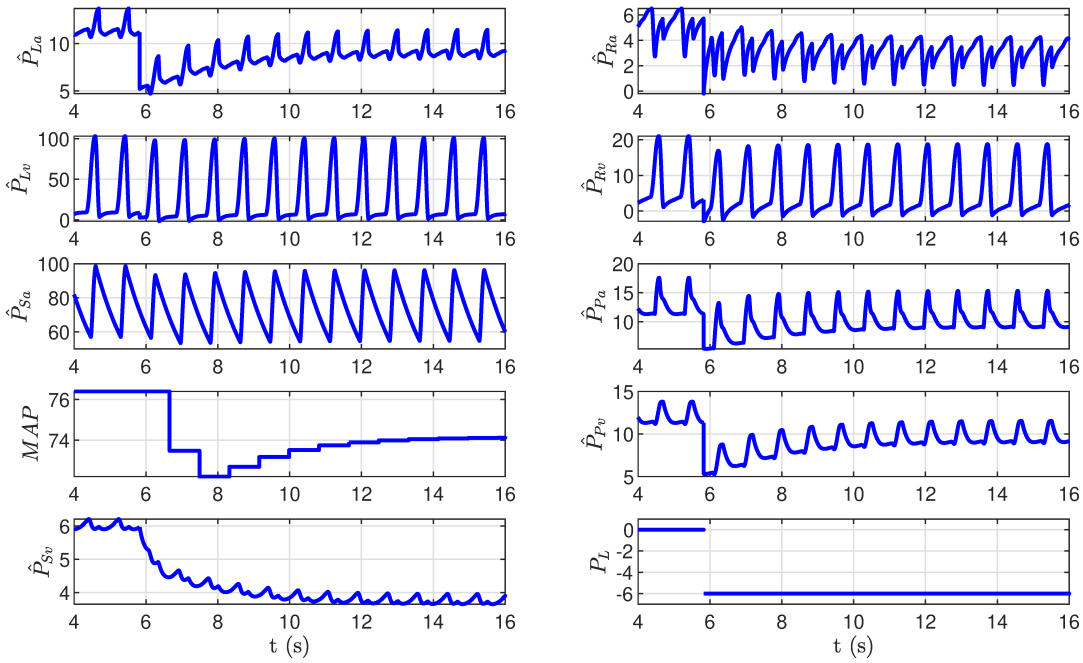

Figure 3.4: The effect of the sudden onset of a constant pleural pressure, P_L on the pressures (in mmHg) in the heart model. Pressures shown are the pressures relative to atmospheric pressure described in equations 2.53 to 2.60, MAP, the mean arterial pressure, is obtained from P_{Sa},the pressure in the systemic artery, with an artificially generated P_L. The onset of pleural pressure causes the heart model to reach a new steady state.

and pressure waves in the heart model. Blood pressure in the compartments relative to atmospheric pressure is approximately in phase with the applied pressure, although with a lag seen mainly in the systemic arteries and veins.

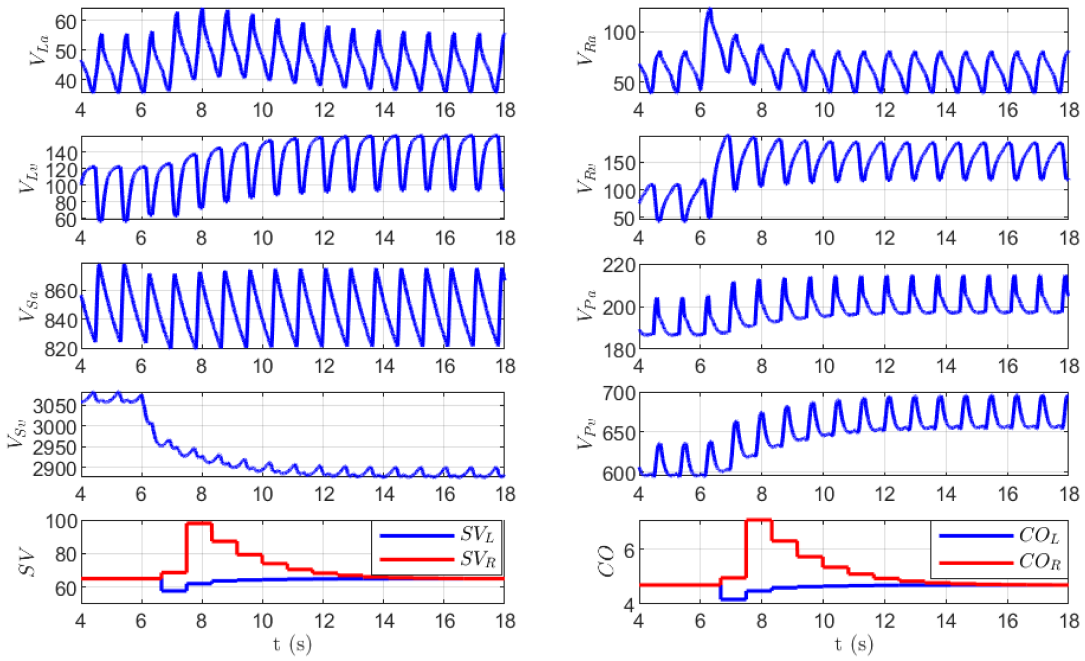

Figure 3.5: The effect of the sudden onset of a constant pleural pressure (the same as Figure 3.4 on the volumes (in mL) in the heart model. Also shown are the stroke volume, SV, (the volume expelled during a heart beat) and the cardiac output, CO, (average blood flow in L/min) of the left and right ventricles. The sudden onset of pleural pressure causes the volumes to reach a new steady state. After initial disturbances, stroke volumes and cardiac outputs return to their initial values.

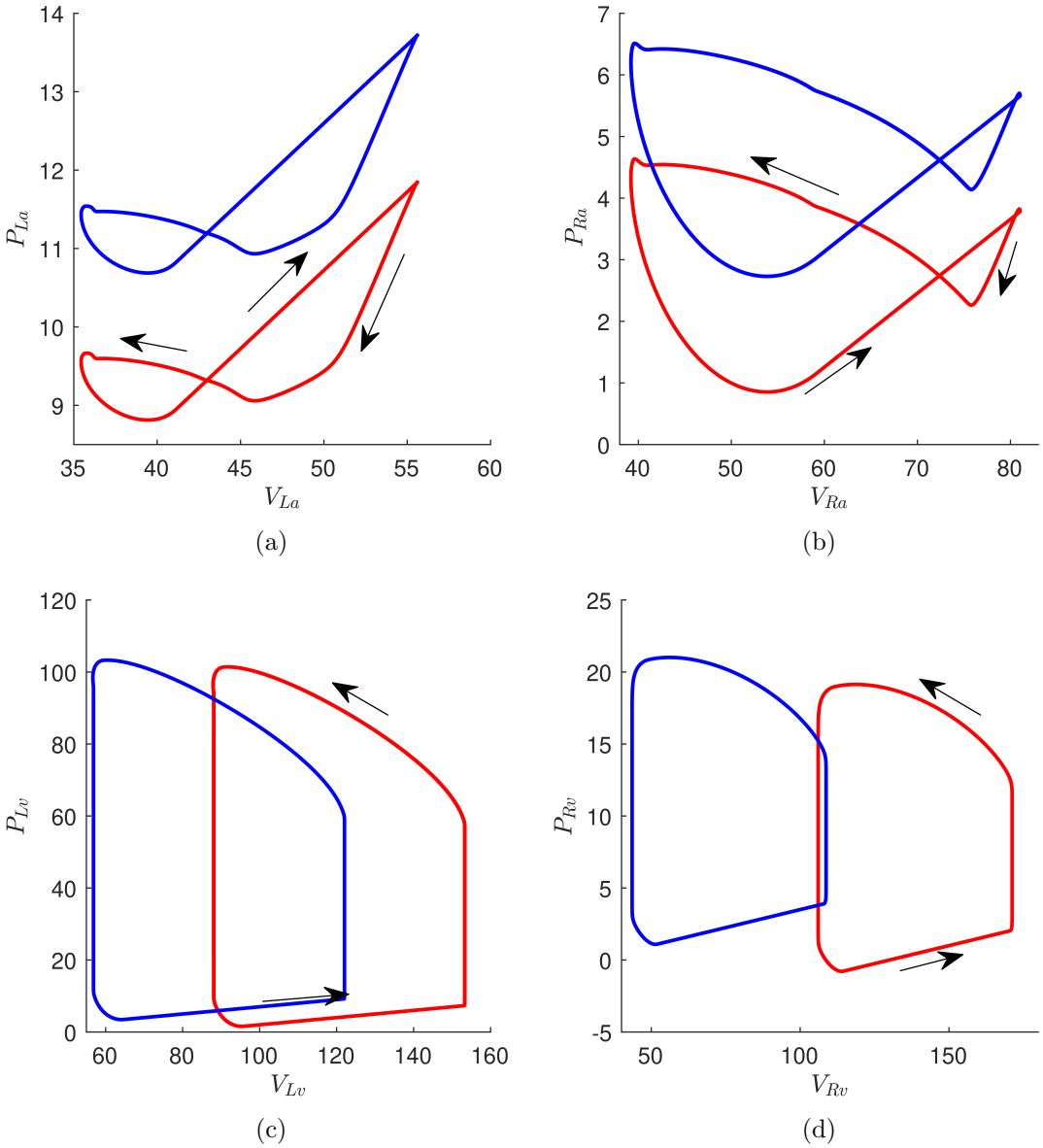

Figure 3.6: P-V loops of left atrium (a), right atrium (b), left ventricle (c) and right ventricle (d) at 72bpm without (blue) and with (red) adjustment by pleural pressure.

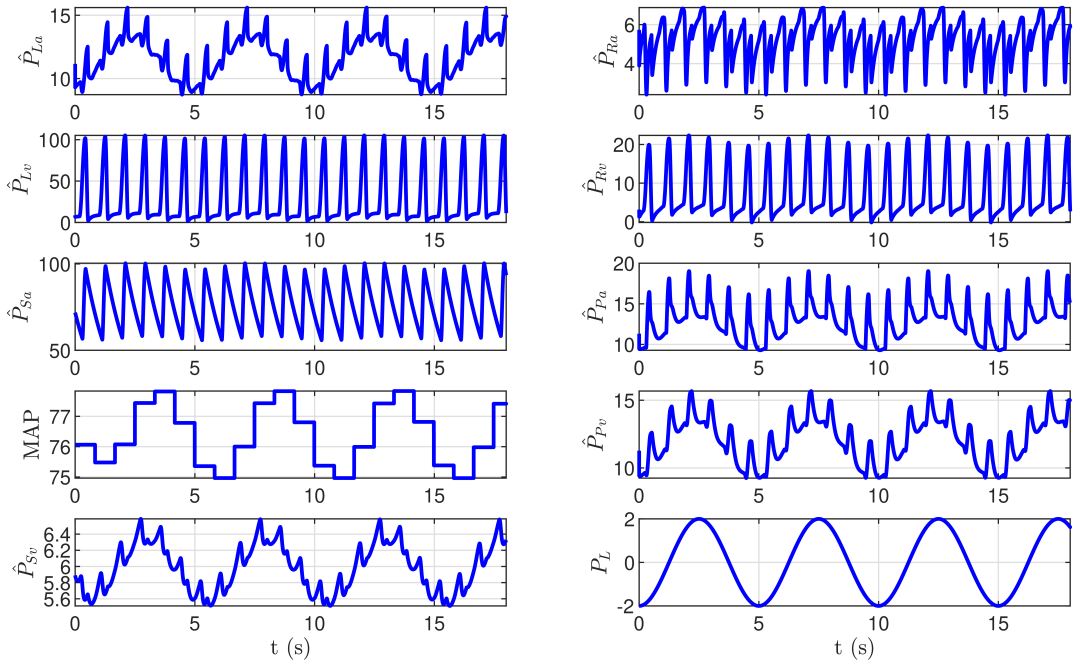

Figure 3.7: Pressures (in mmHg) relative to atmospheric pressure in the heart model with a sine wave pleural pressure input. Pressures in the heart model oscillate when an oscillating pleural pressure is applied. In particular, the oscillations in the *MAP* signal could trigger heart rate variation when blood pressure feedback is included in the HR control model.

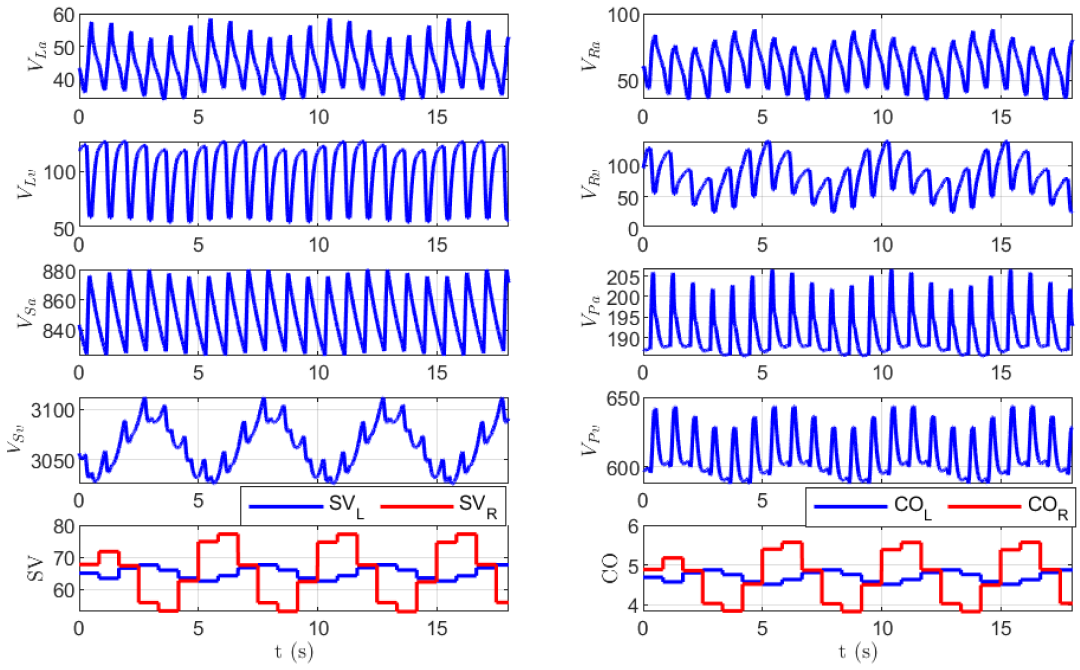

Figure 3.8: Volumes (in mL) in the eight compartments of the heart model with the same oscillating pleural pressure signal as Figure 3.7. Also shown are the stroke volume, SV, (in mL) and the cardiac output, CO, (in L/min) of the left and right ventricles.

3.2.2 Impact of Pulmonary Blood Vessel Resistance

The inclusion of the blood vessel resistance described in section 2.5.2 using equation 2.62 does impact the heart model, but not in a way that changes results significantly. In Figure 3.9 we show two examples where the output of the model is considered with and without a changing blood vessel resistance through different values of k_{Pa} in equation 2.62. Recall that k_{Pa} controls the strength in the change of pulmonary resistance in response to capillary pressure P_{cap}. Negative k_{Pa} ensures that resistance decreases as blood pressure increases.

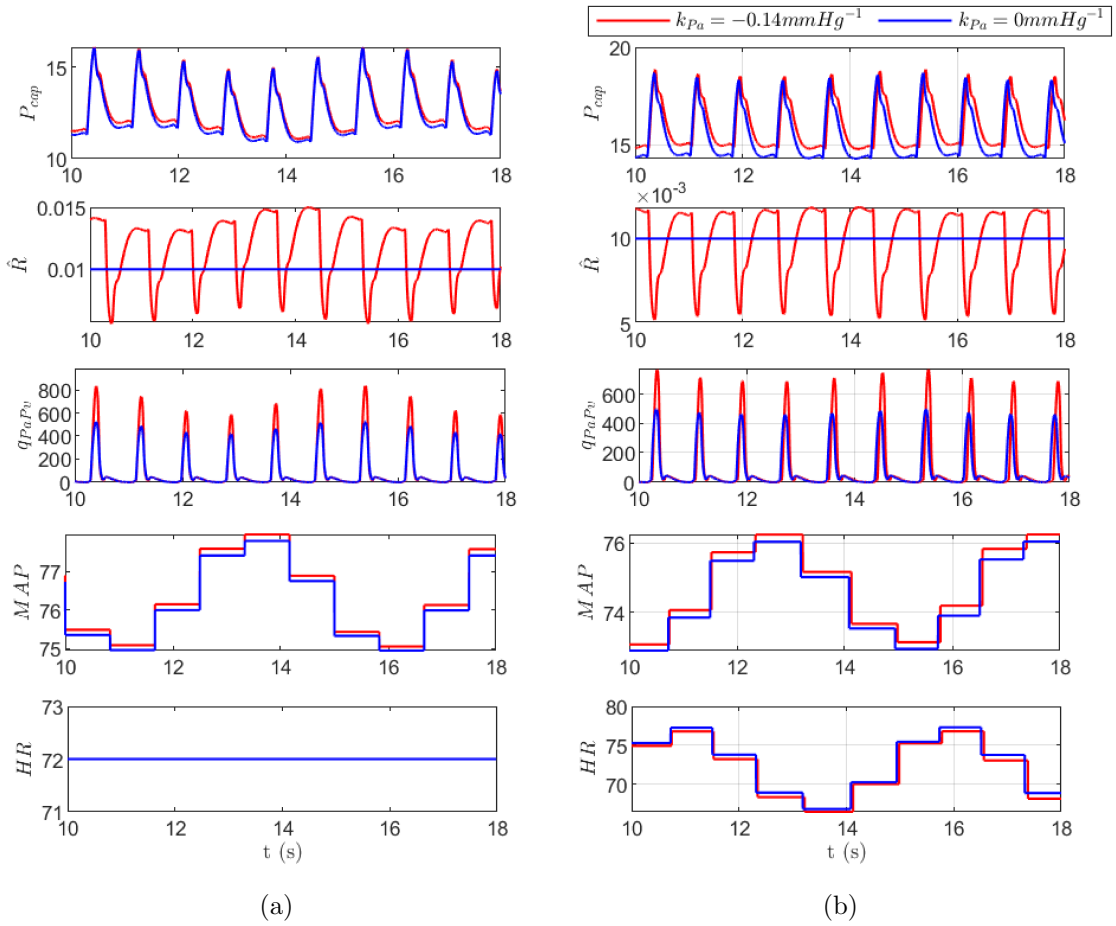

Figure 3.9: Comparison between output with constant and with changing $\hat{R}_{Pa}$ (see Equation 2.62). Shown are P_{cap}, the pressure in the pulmonary capillaries, $\hat{R}_{Pa}$, the pulmonary resistance, q_{PaPv}, the pulmonary blood flow, MAP, mean arterial pressure. In (a), $HR = 72$ bpm is constant and in (b), HR is shown. In these experiments, $P_0 = 14$mmHg, and for constant $\hat{R}_{Pa}$, $k_{Pa} = 0\text{mmHg}^{-1}$, and for changing $\hat{R}_{Pa}$, $k_{Pa} = -0.14\text{mmHg}^{-1}$ When (a) The same oscillating pleural pressure signal as in Figure 3.7 is applied to the heart model at a constant heart rate. (b) Output of the Integrated model with parameters as described in the following chapter. In both cases the introduction of the changing pulmonary resistance does increase oscillation of pulmonary blood flow, but MAP does not change significantly.

Figure 3.9 compares output of the heart model with constant and with variable pulmonary resistance at a constant HR of 72bpm (Figure 3.9a), and with HR control from

the integrated model (Figure 3.9b). We show the capillary pressure (see Equation 2.61), resistance (see Equation 2.62) as a function of capillary pressure, blood flow from the pulmonary arteries to the pulmonary veins (see Equation 2.32), and MAP (see Equation 2.47), HR is also shown for the integrated model. Although pulmonary bloodflow is increased, the effect on capillary pressure is not significant, nor is the effect on MAP.

Figure 3.9b shows selected output of the integrated model with parameters described in Table 2. Two cases are shown, with values of $k_{Pa} = 0, -0.14$. The cases where vascular resistance is constant and non-constant do not give significantly different results for MAP or HR.

Under the current assumptions, the inclusion of variable vascular resistance did not cause a significant change in MAP or HR output. Further work studying the blood vessels of the lungs may yield more significant results, but for the remainder of this thesis, the pulmonary vascular resistance will be left as a constant.

3.3 Summary

In this chapter we showed that the heart model gives physiological levels of blood pressure and volume in the human circulation. We showed the effect of two physical interactions between the the heart and the lungs. Under the assumptions given in section 2.5, a variable pulmonary vascular resistance does not impact the heart model in a way that will affect heart rate control, but the pressure inside the thorax has the potential to impact heart rate through blood pressure feedback. We explore these effects further in Chapter 5.

Chapter 4

Parameter Fitting

The heart rate control model has several parameters which need to be chosen. Where possible we have taken the parameter values from [1], otherwise we set parameters to the same experiments as those used in [1] to allow direct comparison between the original model and the integrated model. In this chapter we show the experiments we used to set parameters for the model and describe how changes in parameters affect the model as a whole.

Table 4.1 gives two sets of parameters and a brief justification; one set with a choice of using P_{Sa} and one with a choice of MAP as the blood pressure signal in the baroreflex.

4.1 Heart Rate Dependance on Arterial Pressure

Experiments which measure the heart rate's response to blood pressure changes inform the choice of parameters affecting the baroreflex. Figure 4.1 shows the baroreflex response to artificially induced changes in blood pressure, experimental data is adapted from [4] and reproduced by our model. The experimental data can be approximated by the curve

$$T_L(MAP) = \frac{A_b}{1 + exp(B_b(MAP - C_b))} + D_b \tag{4.1}$$

where $A_b = 0.5656$, $B_b = \gamma$, $C_b = \delta$, and $D_b = 0.5498$ are constants fitted to the data using the solver "add-in" in Excel. In the HR control model given by equations 2.1 and 2.2, the effect of the baroreceptors can be isolated by setting $c_1 = c_2 = 0$ to remove respiratory modulation and setting $a = 0$ (see Equation 2.3) to remove the respiratory gating. We assume that the steady state behaviour of the model under these conditions must match the experimental data. To replicate the experiment in [4], several levels of constant pleural pressure were applied with only the baroreflex feedback active.

Assuming steady state and the described conditions, we obtain the system

$$0 = -S_1(T_L - T_{L0}) + c_0 C_{VN} - S_M \tag{4.2}$$

$$0 = -S_2(C_{VN} - C_{VN0}) + \frac{c_3}{2} B_R(MAP) \tag{4.3}$$

which can be rearranged to give

$$B_R(MAP) = \frac{2S_2S_1}{c_0c_3}T_L - \frac{2S_2S_1}{c_0c_3}T_{L0} - \frac{2S_2c_0}{c_0c_3}C_{VN0} + \frac{2S_2S_M}{c_0c_3} \tag{4.4}$$

Substituting Equation 4.1 in place of T_L gives

$$\begin{aligned} B_R(MAP) = & \frac{\frac{2A_bS_2S_1}{c_0c_3}}{1+exp(B_b(MAP-C_b))} \\ & + \frac{2D_bS_2S_1}{c_0c_3} - \frac{2S_2S_1}{c_0c_3}T_{L0} - \frac{2S_2c_0}{c_0c_3}C_{VN0} + \frac{2S_2S_M}{c_0c_3} \end{aligned} \tag{4.5}$$

Matching the form of Equation 4.5 to Equation 2.4 requires

$$\frac{2A_bS_1S_2}{c_0c_3} = 1 \tag{4.6}$$

which gives a relationship between experimental data and the parameters S_1, S_2 and c_3 (c_0 is assumed to be the same as [1]).

Figure 4.1 shows output of the integrated model when only the baroreflex is influencing heart rate and the pleural pressure provides a change to mean arterial pressure. Parameters were chosen using Equation 4.6. This relationship holds, as seen in Figure 4.1, when either MAP (Eq. 2.5) or P_{Sa} (Eq. 2.6) is used as the pressure signal in the linearised baroreflex and provides a constraint on the parameters which is useful in the following section.

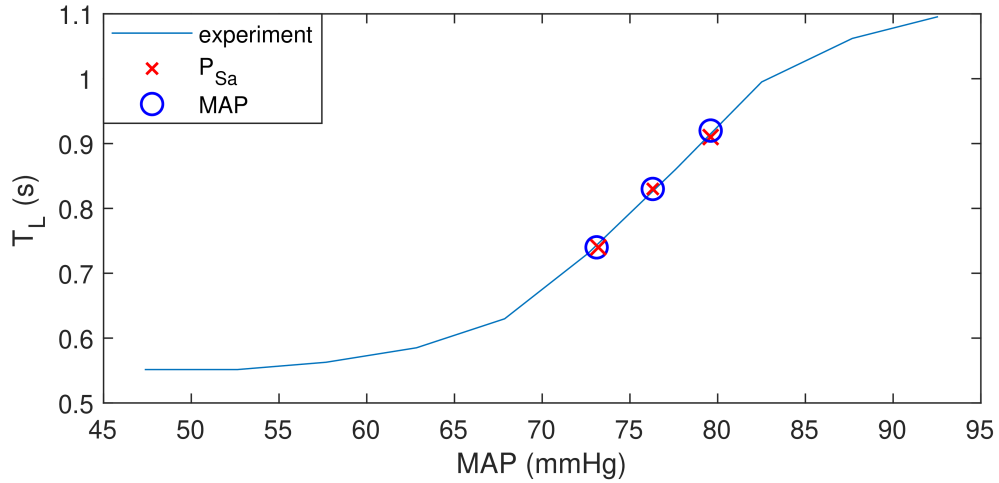

Figure 4.1: Heart period, T_L, as a function of mean arterial pressure, MAP, approximates the linear region of data adapted from [4]. We shifted the midpoint of the data to coincide with the MAP of the heart model at 72bpm. Respiratory modulation is removed by setting $c_1 = c_2 = 0$. Constant $P_L = -15, 0, 15$ mmHg are applied to the heart model and the integrated model is allowed to reach steady state. C_{VN0} is set with two values, $C_{VN0} = 1.24$ when MAP is used in Equation 2.5, and $C_{VN0} = 1.18$ when P_{Sa} is used in Equation 2.6 such that when $P_L = 0$, $MAP = 76.1$ mmHg at a heart rate of 72bpm. The baroreflex used is the linear baroreflex.

4.2 Fitting Other Parameters

Experiments which measure RSA amplitude at different respiratory frequencies show that RSA amplitude peaks at a certain respiratory frequency [5]. The model in [1] was able to replicate this behaviour. Here we fit the integrated model to the results produced in [1]. $S_1 = S_2$ was adjusted to ensure that the peak amplitude of RSA occured at 7 breaths per minute, and c_3 was changed to satisfy Equation 4.6. Using the parameters given in Table 4.1 the integrated model has a maximum RSA amplitude ($T_L^{max} - T_L^{min}$) of approximately 0.31s at a respiratory frequency of 7 breaths per minute. The integrated model using P_{Sa} in the baroreflex gives good agreement with [1].

4.3 Summary

In this section we showed that parameters in the integrated model can be chosen to fit experimental results. Using P_{Sa} as the blood pressure signal in the baroreflex gives better agreement with the model in [1] than using MAP.

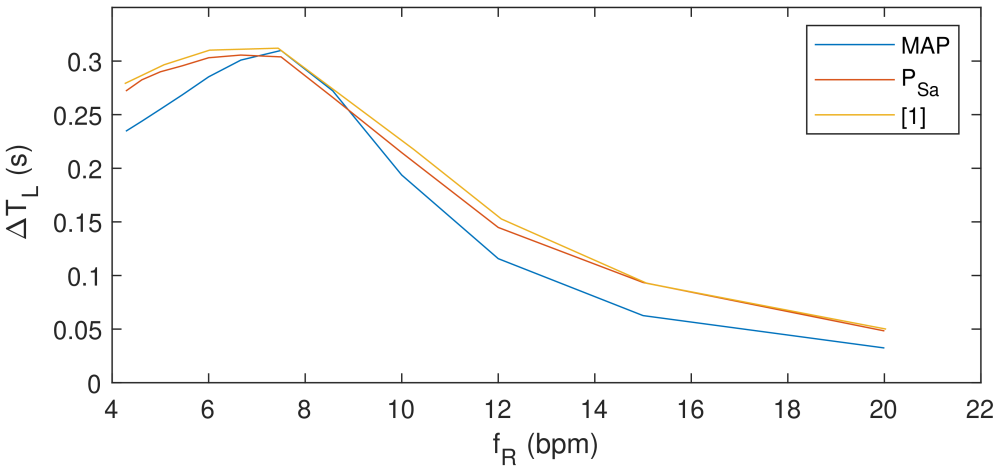

(a)

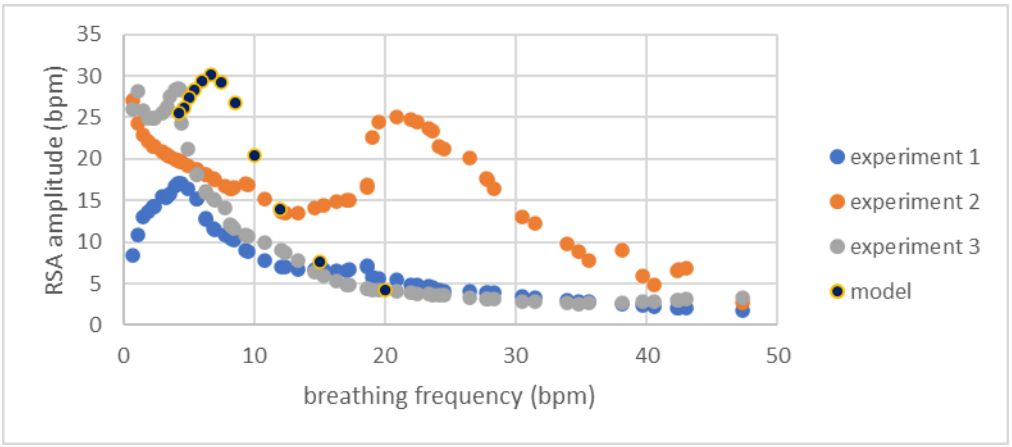

(b)

Figure 4.2: (a) RSA peaks at a low respiratory frequency. Parameters can be chosen in the integrated model to give good agreement with the results in [1] whether *MAP* (Eq. 2.5) or P_{Sa} (Eq. 2.6) is chosen as the source of blood pressure in the Equation 2.5 . Tidal volume is held at 1L. RSA amplitude is plotted against respiratory frequency, f_R. Using P_{Sa} as the pressure signal in the baroreflsex gives better agreement with the previous model in [1].
(b) Model output with P_{Sa} in the baroreflex (Eq. 2.6) in the same experiment as Fig. 4.2a, compared with experimental results. Experiments 1 and 3: [5], experiment 2: [6]. It is evident that there is a variety of peak RSA amplitudes and breathing frequencies present between different patients. While in principle we could match parameters with any of the experiments here, we chose to match the results in [1].

Table 4.1: Parameters for the model of heart rate control for humans. When units are not shown, the parameters are dimensionless. All parameter-fittings were done with the linear baroreflex.

Parameter	Value	Justification
S_1	1.0677 Hz	fits RSA peak amplitude at ≈7 breaths per minute with MAP in Eq. 2.5
	0.81 Hz	fits RSA peak amplitude at ≈7 breaths per minute with P_{Sa} in Eq. 2.5
		increasing S_1, S_2, c_3 according to Equation 4.6 reduces peak RSA amplitude and increases respiratory frequency for peak RSA
S_2		assumed to be the same as S_1 see note in S_1
T_{L0}	0.6 s	[1]
c_0	1	[1]
S_M	1	[1]
C_{VN0}	1.65	gives mean HR with MAP in B_R
	1.6	gives mean HR with P_{Sa} in B_R
c_1	1.45 Hz	fits RSA peak amplitude of ≈ 0.3s with MAP in Eq. 2.5
	1.18 Hz	fits RSA peak amplitude of ≈ 0.3s with P_{Sa} in Eq. 2.5
		Increasing c_1 increases peak RSA amplitude and increases mean HR
c_2	0.05 $(\text{sL})^{-1}$	[1] Increasing c_2 increases dependance of RSA amplitude on lung volume and reduces mean HR
k_2	4.2 L	[1]
c_3	1.29 Hz	fitted to data in figure 4.1 with MAP in Eq. 2.5
	0.74 Hz	fitted to data in figure 4.1 with P_{Sa} in Eq. 2.5 see note in S_1
γ	-0.1945 mmHg^{-1}	[1]
δ	76.1 mmHg	MAP at 72 bpm in the heart model
a	4 s/L	[1]

Chapter 5

Model and Hypothesis Testing

In this chapter we verify further the integrated model's qualitative agreement with results from the model in [1]. We show the relationship between RSA amplitude and breathing frequency, and the phase between the peak in the heart period and the preceding trough in lung volume. We also use the model to address the discussion over whether RSA is caused by baroreflex response to blood pressure changes induced by breathing or whether the phenomenon is centrally modulated. We conclude that the baroreflex alone is insufficient to cause the amplitude of HR change required for RSA. We also test the hypothesis that RSA minimises heart energy consumption while maintaining arterial CO_2 levels. The results from the integrated model do not agree with those found in [1] and point to a need to investigate the model and the calculation further.

5.1 Appearance of RSA

Figure 5.1 shows $V_A(t)$, $HR(t)$, and $C_{VN}(t)$ as calculated by the integrated model while keeping minute ventilation (the volume of air inhaled in a minute) a constant. In both cases presented, taking MAP (see Equation 2.5) or taking P_{Sa} (see Equation 2.6) as the pressure source in the baroreflex, deep, slow breathing increases RSA amplitude and fast, shallow breathing reduces it, an outcome which is retained from the model in [1].

For breathing frequencies f_R in the range 4 breaths per minute to 20 breaths per minute, the phase, which we define as being between a trough in volume and a peak in the heart period, between heart beat period and lung volume agrees closely with results in [1] (See Figure 5.2).

5.2 Source of RSA

Some investigators believe that RSA is due to direct central modulation of the parasympathetic nerves, while others believe that RSA is caused by the baroreflex response to pressure oscillations in the thorax causing blood pressure osscilations. We can address this controversy by comparing the integrated model to outcomes generated by setting $c_1 = c_2 = 0$ so only the baroreflex remains to affect the heart rate through influence from the pleural pressure.

Figure 5.3 shows RSA amplitude when only the baroreflex influences the heart rate. Contrasted with Figure 4.2, the RSA amplitudes seen here are very small, suggesting that

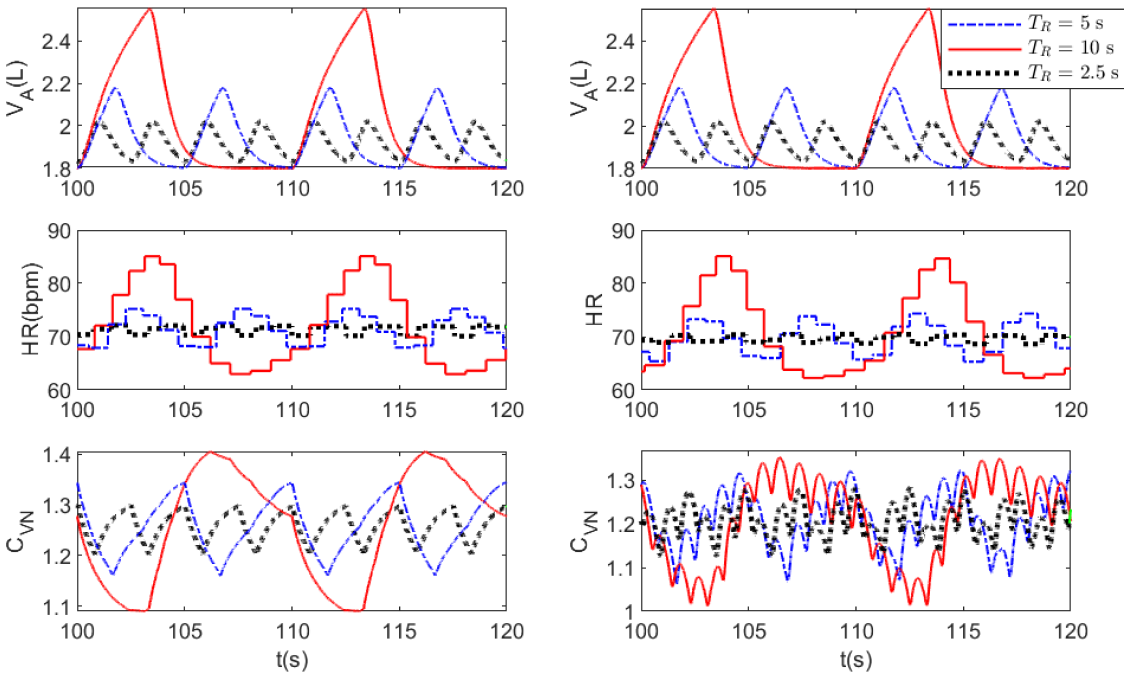

(a) (b)

Figure 5.1: RSA amplitude is largest under deep slow breathing in either the case where MAP (a) or P_{Sa} (b) is taken as the pressure signal in the baroreflex. Panels from top to bottom: lung volume V_A, at breathing period $T_R = 2.5, 5, 10$s adjusted to keep minute ventilation constant, heart rate HR, and vagal nerve activity C_{VN}.

the baroreflex alone is insufficient to triggure RSA at physiological levels, supporting the main assumption in [1] that central respiratory modulation of the vagal nerve is responsible for most of the amplitude of RSA.

Figure 5.4 compares RSA amplitudes when some aspects of the integrated model have been removed. When the baroreflex is removed, there is no peak in RSA amplitude, which instead keeps rising as breathing frequency decreases, suggesting that the baroreflex is responsible for the reduction in amplitude, as suggested in [1]. When the influence of pleural pressure was removed, mean heart rate decreased. This was because the constant component of the pleural pressure reduces blood pressure, which the baroreflex responds to by increasing heart rate. In Fig. 5.4 we increased mean heart rate to be the same as in the full model to correct for the impact of the constant component of the pleural pressure, and repeated the experiment varying F_R. P_L contributes a small amount to the amplitude of RSA.

5.3 Physiological Significance of RSA

It has been hypothesised in [1, 19] that RSA optimises the energy used by the heart while maintaining physiological levels of arterial CO_2, both found a clear minimum in energy consumption at physiological levels of RSA. In [1], RSA amplitude was adjusted while mean arterial CO_2 in a breathing period was kept constant. The parameter c_0 was

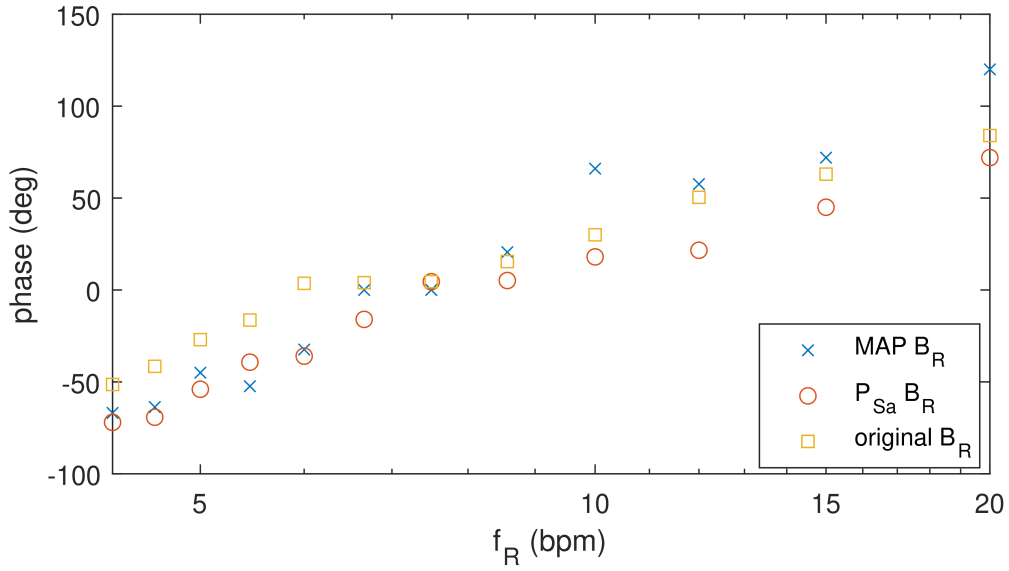

Figure 5.2: Phase between a trough in V_A and the preceding peak in T_L. The results in the integrated control model are in qualitative agreement with the original model in [1]. Simulations were done with the linear baroreflex, $T_I = T_E$, and $V_T = 1L$. The corresponding experiment in [1] extended to higher f_R, the implementation used for this figure did not allow V_T to be held at 1L across the whole range.

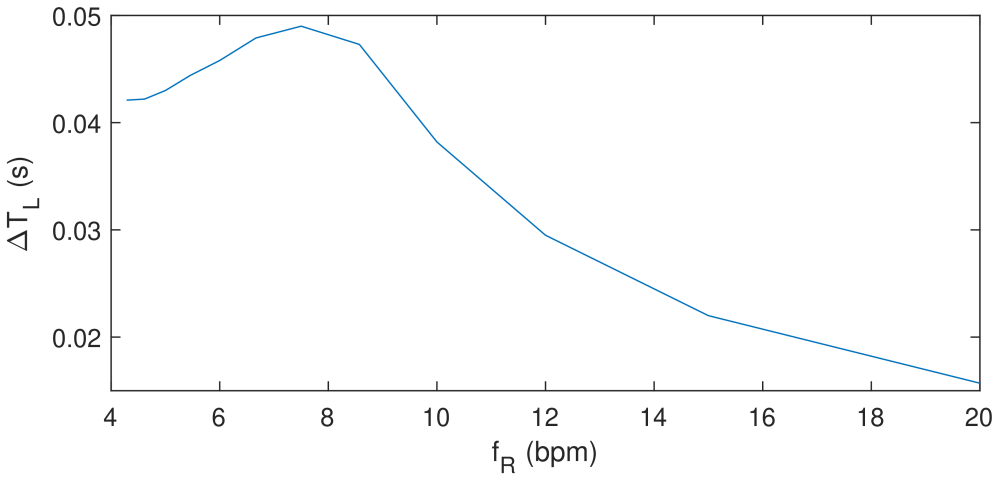

Figure 5.3: RSA amplitude with changing breathing frequency when only the baroreflex affects the vagus nerve. Blood pressure changes are induced by pleural pressure applied to the heart model. P_{Sa} is the pressure signal in the baroreflex. $c_1 = c_2 = 0$, $V_T = 1L$ and $T_I = T_E$ for all points. Compared with Figure 4.2, the amplitude of RSA caused by blood pressure oscillations is small when only the baroreflex feedback affects the heart rate.

decreased from 1 to 0 and S_M reduced with it to maintain CO_2 levels. The energy over a breath was calculated from the heart rate using the integral

$$E = V_C^2 R_S \int_0^{T_R} HR^2 dt \tag{5.1}$$

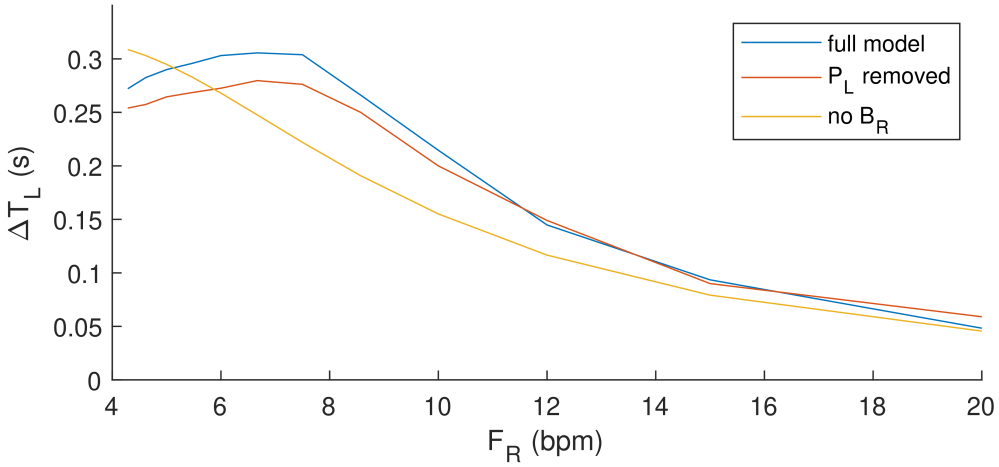

Figure 5.4: Here we compare model output with P_{Sa} in the baroreflex (full model) to the effects of removing P_L in the heart model and of removing the baroreflex . This is the same experiment as in Figure 4.2. When removing P_L, $C_{VN0} = 1.55$ to keep the mean HR near that of the full model. The inclusion of P_L contributes a small amount to the amplitude of RSA. When the baroreflex is removed, the breathing frequency of maximum RSA moves to the left.

where V_C, the stroke volume, and R_S, the systemic vascular resistance were estimated constants.

We can perform a similar experiment with the integrated model, but rather than integrating energy from the heart rate, we can calculate work done on the blood using pressure and volume in the left ventricle. Assuming that no work other than fluid work is done and that pressure is distributed evenly in a container, work done by a fluid during a volume change from V_A to V_B is given by [49]

$$W = \int_{V_A}^{V_B} P dV \tag{5.2}$$

We have $P(t)$ and $\frac{dV(t)}{dt}$ for the left ventricle, which we can substitute into equation 5.2 to obtain the integral

$$W = \int_{t_a}^{t_b} P(t) \frac{dV(t)}{dt} dt \tag{5.3}$$

giving the work done by the blood over a period of time $t_a \leq t \leq t_b$ in units of mmHg·mL, which can be converted to Joules by the relation $c_j$mmHg·mL=Pa·m^3, where $c_j = 0.000133322$.

The following integral gives the work done on the blood by a compartment during a breath

$$W_{T_R} = -c_j \int_0^{T_R} P(\tau) \frac{dV(\tau)}{d\tau} d\tau \tag{5.4}$$

where $\tau = t - t_s$ and t_s is the start time of the breath of interest. Note that this is the

negative of the work done by the blood in Equation 5.3.

Integrating Eq. 5.4 presents inconsistency in the work done over one breath since the end of a heartbeat and the end of a breath rarely coincide. To overcome this we find the average energy over 20 breaths and use the integral

$$W_{T_{20}} = -c_j \int_{t_{s1}}^{t_{s2}} P(t) \frac{dV(t)}{dt} dt \tag{5.5}$$

where t_{s1} is the start time of the first heart beat after the first breath, and t_{s2} is the start time of the first heart beat after the last breath. The average energy in one breath is calculated by taking the average power over this time period and multiplying by T_R to give a more consistent averaged energy consumption over a single breath.

$$W_{T_R} = T_R \frac{W_{T_{20}}}{t_{s2} - t_{s1}} \tag{5.6}$$

The experiment we present here differs slightly from [1]. We found that the choice of stroke volume, V_C, in the lung model to be non-constant gave different results than choosing it to be constant. We took a breathing period $T_R = 10s$ with equal inspiration and expiration times and kept $\bar{p}_{ce} = 38.05 \pm 0.02$. As the starting value in the experiments we chose $c_0 = 0.2$ and $S_M = 0.045$ to give a mean heart rate around 72bpm and therefore the same initial heart power. c_0 was increased in increments of 0.1, and S_M adjusted with it to keep $\bar{p}_{ce} = 38.05 \pm 0.02$. For $c_0 < 0.2$, S_M took on an unphysiological negative value in order to maintain $\bar{p}_{ce}$. V_C, the volume of blood pumped into the lungs in a heartbeat was taken as either a constant or directly measured in the heart model. We used the values, $k_n = 0.16$, $V_T \approx 1L$ in the experiment with a constant stroke volume, and $k_n = 0.17$ in the experiment with a non constant stroke volume to make sure that the levels of arterial CO_2 are the same in both experiments. In the case of constant V_C, we attained qualitatively similar results to [1] where there is an RSA amplitude that minimizes energy consumption, however the change in energy consumption to maintain $\bar{p}_{ce}$ as RSA amplitude is varied, is insignificant, and the minimum $\bar{p}_{ce}$ occurs with an RSA amplitude of 4 breaths per minute, compared to 12 breaths per minute in [1]. In the case of the non constant V_C, there is an RSA amplitude which maximizes energy consumption, in contrast to the hypothesis in [1, 19].

The experiments in Figure 5.5 indicate that the inclusion of a variable stroke volume in the lung model appears to flip the overall trend from [1] that a particular value of RSA minimises work done by the heart. This result will be the subject of further investigation. It might be that the integral in Equation 5.3 needs rethinking. Specifically in Equation 5.1 the energy was calculated only during ventricular contraction and not through the whole cycle of ventricular contraction and ventricular refilling. It is also possible that changing the stroke volume violated some assumptions in the lung model and further changes in this model are necessary in compensation.

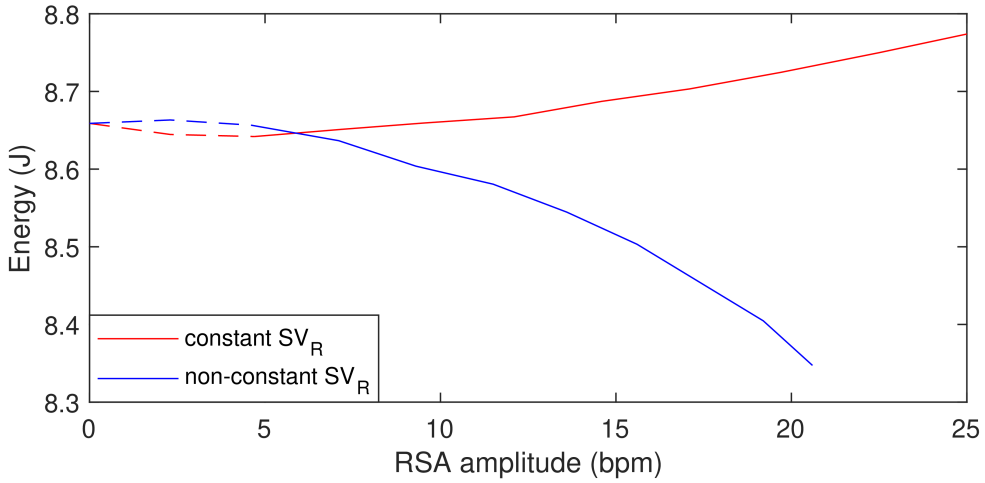

Figure 5.5: RSA amplitude changes the work done by the heart, as calculated by Equation 5.6, to maintain arterial CO_2 levels. Taking the non-constant stroke volume from the heart model in the lung model appears to produce a maximum in the energy consumption, opposite to the case in [1]. In this experiment c_0 is varied and S_M is adjusted in order to maintain a mean CO_2 level. Dashed lines indicate a negative S_M for completeness.

Chapter 6

Conclusion

In this thesis we coupled together three models: a model of heart and circulation, a model of heart rate control, and a model of the lungs which had previously been included in the heart rate control model. In including the heart model we were able to apply heart rate control to the heart model as a replacement for preset heart rate variation, use measured rather than estimated blood pressure in baroreceptor feedback to the parasympathetic nerve, and account for the influence of pleural pressure on the heart. Although the heart model we used was chosen because of its ability to represent heart function for a large range of heart rates, the changes introduced could be used to couple other heart models with the HR control model. We showed that the model can reproduce experimental data involving the heart rate response to blood pressure and the amplitude of RSA, and found a relationship between parameters in the HR control model to simultaneously match such experiments. Fitting of parameters in the lung and heart models was beyond the scope of the thesis and a sensitivity analysis of the results to changes in parameters will need to be done in the future. The model demonstrated that the baroreflex is unable to cause significant heart rate oscillations in response to changes in pleural pressure, and that the main source of RSA is direct central respiratory modulation of the heart rate. The model did not replicate previous results showing that RSA minimises the work done by the heart while maintaining blood CO_2 levels. This indicates that more work is needed to understand the effect of a variable stroke volume on the lungs as well as looking carefully at how the energy of the heart was calculated.

Bibliography

[1] A. Ben-Tal, S. S. Shamailov, and J. F. R. Paton, "Central regulation of heart rate and the appearance of respiratory sinus arrhythmia: New insights from mathematical modeling," *Mathematical Biosciences*, vol. 255, pp. 71–82, 2014.

[2] A. Ben-Tal, "Simplified models for gas exchange in the human lungs," *Journal of Theoretical Biology*, vol. 238, no. 2, pp. 474–495, 2006.

[3] A. Ben-Tal and J. C. Smith, "A model for control of breathing in mammals: Coupling neural dynamics to peripheral gas exchange and transport," *Journal of Theoretical Biology*, vol. 251, no. 3, pp. 480–497, 2008.

[4] F. Lador, E. Tam, M. Azabji Kenfack, M. Cautero, C. Moia, D. R. Morel, C. Capelli, and G. Ferretti, "Phase I dynamics of cardiac output, systemic O_2 delivery, and lung O_2 uptake at exercise onset in men in acute normobaric hypoxia," *American Journal of Physiology-Regulatory, Integrative and Comparative Physiology*, vol. 295, no. 2, pp. R624–R632, 2008.

[5] J. A. Hirsch and B. Bishop, "Respiratory sinus arrhythmia in humans: how breathing pattern modulates heart rate," *American Journal of Physiology-Heart and Circulatory Physiology*, vol. 241, no. 4, pp. H620–H629, 1981.

[6] A. Angelone and N. A. Coulter, "Respiratory sinus arrhythmia: a frequency dependent phenomenon," *Journal of Applied Physiology*, vol. 19, no. 3, pp. 479–482, 1964.

[7] L. Sherwood, *Human physiology : from cells to systems.* West Pub. Co., 1993.

[8] P. Grossman and E. W. Taylor, "Toward understanding respiratory sinus arrhythmia: Relations to cardiac vagal tone, evolution and biobehavioral functions," *Biological Psychology*, vol. 74, no. 2, pp. 263 – 285, 2007. Special Issue of Biological Psychology on Cardiac Vagal Control, Emotion, Psychopathology, and Health.

[9] E. L. O'Callaghan, R. M. Lataro, E. L. Roloff, A. S. Chauhan, H. C. Salgado, E. Duncan, A. Nogaret, and J. F. Paton, "Enhancing respiratory sinus arrhythmia increases cardiac output in rats with left ventricular dysfunction," *The Journal of Physiology*, vol. 598, no. 3, pp. 455–471, 2020.

[10] S. Noreen, A. Ben-Tal, M. Elstad, W. Sweatman, R. Ramchandra, and J. Paton, "Mathematical modelling of atrial and ventricular pressure-volume dynamics and their change with heart rate," *Mathematical Biosciences*, 2021. Submitted for publication.

[11] G. J. Tortora and B. Derrickson, *Principles of anatomy and physiology*. Wiley, 14 ed., 2014.

[12] P. Larsen, Y. Tzeng, P. Sin, and D. Galletly, "Respiratory sinus arrhythmia in conscious humans during spontaneous respiration," *Respiratory Physiology & Neurobiology*, vol. 174, no. 1-2, pp. 111–118, 2010.

[13] J. M. Karemaker, "Last Word on Point: Counterpoint: Respiratory sinus arrhythmia is due to a central mechanism vs. respiratory sinus arrhythmia is due to the baroreflex mechanism," *Journal of Applied Physiology*, vol. 106, no. 5, p. 1750, 2009.

[14] D. L. Eckberg, "Point: Counterpoint: Respiratory sinus arrhythmia is due to a central mechanism vs. respiratory sinus arrhythmia is due to the baroreflex mechanism," *Journal of Applied Physiology*, vol. 106, no. 5, pp. 1740–1742, 2009.

[15] J. M. Karemaker, "Counterpoint: Respiratory sinus arrhythmia is due to the baroreflex mechanism," *Journal of Applied Physiology*, vol. 106, no. 5, pp. 1742–1743, 2009. PMID: 19414625.

[16] C. Julien, "Comments on Point: Counterpoint: Respiratory sinus arrhythmia is due to a central mechanism vs. respiratory sinus arrhythmia is due to the baroreflex mechanism RSA: Numbers and Beyond," *Journal of Applied Physiology*, vol. 106, no. 5, p. 1745, 2009.

[17] M. Elstad, L. Walløe, N. L. Holme, E. Maes, and M. Thoresen, "Respiratory sinus arrhythmia stabilizes mean arterial blood pressure at high-baroCurve interval in healthy humans," *European Journal of Applied Physiology*, vol. 115, no. 3, pp. 521–530, 2015.

[18] J. Hayano, F. Yasuma, A. Okada, S. Mukai, and T. Fujinami, "Respiratory sinus arrhythmia - Phenomenon improving pulmonary gas exchange and circulatory efficiency," *Circulation*, vol. 94, no. 4, pp. 842–847, 1996.

[19] A. Ben-Tal, S. Shamailov, and J. Paton, "Evaluating the physiological significance of respiratory sinus arrhythmia: looking beyond ventilation–perfusion efficiency," *The Journal of Physiology*, vol. 590, no. 8, pp. 1989–2008, 2012.

[20] H. R. Warner and A. Cox, "A mathematical model of heart rate control by sympathetic and vagus efferent information," *Journal of Applied Physiology*, vol. 17, no. 2, pp. 349–355, 1962.

[21] T. Pickering, B. Gribbin, E. S. Petersen, D. Cunningham, and P. Sleight, "Effects of autonomic blockade on the baroreflex in man at rest and during exercise," *Circulation Research*, vol. 30, no. 2, pp. 177–185, 1972.

[22] D. G. Farmer, M. Dutschmann, J. F. Paton, A. E. Pickering, and R. M. McAllen, "Brainstem sources of cardiac vagal tone and respiratory sinus arrhythmia," *The Journal of Physiology*, vol. 594, no. 24, pp. 7249–7265, 2016.

[23] C. Menuet, A. A. Connelly, J. K. Bassi, M. R. Melo, S. Le, J. Kamar, N. N. Kumar, S. J. McDougall, S. McMullan, and A. M. Allen, "Prebötzinger complex neurons drive

respiratory modulation of blood pressure and heart rate," *Elife*, vol. 9, p. e57288, 2020.

[24] A. E. Simms, J. F. Paton, and A. E. Pickering, "Hierarchical recruitment of the sympathetic and parasympathetic limbs of the baroreflex in normotensive and spontaneously hypertensive rats," *The Journal of Physiology*, vol. 579, no. 2, pp. 473–486, 2007.

[25] M. Kollai and K. Koizumi, "Cardiac vagal and sympathetic nerve responses to baroreceptor stimulation in the dog," *Pflügers Archiv*, vol. 413, no. 4, pp. 365–371, 1989.

[26] C. M. Heesch, "Reflexes that control cardiovascular function," *Advances in Physiology Education*, vol. 277, no. 6, p. S234, 1999.

[27] C. H. Davos, L. C. Davies, and M. Piepoli, "The effect of baroreceptor activity on cardiovascular regulation," *Hellenic Journal of Cardiology*, vol. 43, no. 145, p. 55, 2002.

[28] B. Haymet and D. McCloskey, "Baroreceptor and chemoreceptor influences on heart rate during the respiratory cycle in the dog," *The Journal of Physiology*, vol. 245, no. 3, pp. 699–712, 1975.

[29] S. Magder, "Heart-lung interaction in spontaneous breathing subjects: the basics," *Annals of Translational Medicine*, vol. 6, no. 18, 2018.

[30] J. F. Jallon, E. Abdulhay, P. Calabrese, P. Baconnier, and P.-Y. Gumery, "A model of mechanical interactions between heart and lungs," *Philosophical Transactions of the Royal Society A: Mathematical, Physical and Engineering Sciences*, vol. 367, no. 1908, pp. 4741–4757, 2009.

[31] R. Beyar, S. Sideman, and U. Dinnar, "Cardiac assist by intrathoracic and abdominal pressure variations: a mathematical study," *Medical and Biological Engineering and Computing*, vol. 22, no. 6, pp. 507–515, 1984.

[32] Y. Goldstein, R. Beyar, and S. Sideman, "Influence of pleural pressure variations on cardiovascular system dynamics: a model study," *Medical and Biological Engineering and Computing*, vol. 26, no. 3, pp. 251–259, 1988.

[33] E. B. Randall, A. Billeschou, L. S. Brinth, J. Mehlsen, and M. S. Olufsen, "A model-based analysis of autonomic nervous function in response to the Valsalva maneuver," *Journal of Applied Physiology*, vol. 127, no. 5, pp. 1386–1402, 2019.

[34] M. S. Olufsen, H. T. Tran, J. T. Ottesen, L. A. Lipsitz, and V. Novak, "Modeling baroreflex regulation of heart rate during orthostatic stress," *American Journal of Physiology-Regulatory, Integrative and Comparative Physiology*, vol. 291, no. 5, pp. R1355–R1368, 2006.

[35] J. T. Ottesen, "Modelling the dynamical baroreflex-feedback control," *Mathematical and Computer Modelling*, vol. 31, no. 4-5, pp. 167–173, 2000.

[36] J. T. Ottesen and M. S. Olufsen, "Functionality of the baroreceptor nerves in heart rate regulation," *Computer Methods and Programs in Biomedicine*, vol. 101, no. 2, pp. 208–219, 2011.

[37] T. Buchner, "A quantitative model of relation between respiratory-related blood pressure fluctuations and the respiratory sinus arrhythmia," *Medical & Biological Engineering & Computing*, vol. 57, no. 5, pp. 1069–1078, 2019.

[38] D. C. McLernon, N. J. Dabanloo, A. Ayatollahi, V. J. Majd, and H. Zhang, "A new nonlinear model for generating RR tachograms," in *Computers in Cardiology, 2004*, pp. 481–484, 2004.

[39] M. Barbi, A. Di Garbo, and R. Balocchi, "Improved integrate-and-fire model for RSA," *Mathematical Biosciences and Engineering*, vol. 4, no. 4, pp. 609–616, 2007.

[40] J. Christen, G. Ruiz, and J. Torres, "Respiratory sinus arrhythmia from two coupled pacemakers," *Biosystems*, vol. 61, no. 1, pp. 27–32, 2001.

[41] F. Dexter, Y. Rudy, M. N. Levy, and E. N. Bruce, "Mathematical model of cellular basis for the respiratory sinus arrhythmia," *Journal of Theoretical Biology*, vol. 150, no. 2, pp. 157–173, 1991.

[42] S. Hirabayashi and M. Iwamoto, "Emotion, respiration, and heart rate variability: A mathematical model and simulation analyses," *Applied Sciences*, vol. 9, no. 23, p. 5008, 2019.

[43] R. Negoescu and I.-E. Csiki, "Model of respiratory sinus arrhythmia in man," *Medical and Biological Engineering and Computing*, vol. 27, no. 3, pp. 260–268, 1989.

[44] H. G. Borst, M. Mcgregor, J. L. Whittenberger, and E. Berglund, "Influence of pulmonary arterial and left atrial pressures on pulmonary vascular resistance," *Circulation Research*, vol. 4, no. 4, pp. 393–399, 1956.

[45] S. Permutt, B. Bromberger-Barnea, and H. Bane, "Alveolar pressure, pulmonary venous pressure, and the vascular waterfall," *Respiration*, vol. 19, no. 4, pp. 239–260, 1962.

[46] M. Elstad, E. L. O'Callaghan, A. J. Smith, A. Ben-Tal, and R. Ramchandra, "Cardiorespiratory interactions in humans and animals: rhythms for life," *American Journal of Physiology-Heart and Circulatory Physiology*, vol. 315, no. 1, pp. H6–H17, 2018.

[47] J. E. Hall, *Guyton and Hall textbook of medical physiology. [electronic resource].* Elsevier, 2016.

[48] M. Kawasaki, R. Tanaka, K. Ono, S. Minatoguchi, T. Watanabe, M. Iwama, T. Hirose, M. Arai, T. Noda, S. Watanabe, M. R. Zile, and S. Minatoguchi, "A novel ultrasound predictor of pulmonary capillary wedge pressure assessed by the combination of left atrial volume and function: A speckle tracking echocardiography study," *Journal of Cardiology*, vol. 66, no. 3, pp. 253–262, 2015.

[49] D. Giancoli, *Physics for scientists & engineers with modern physics.* Upper Saddle River, N.J: Pearson Prentice Hall, 4 ed., 2009.